Inorganic Chemistry

pubs.acs.org/IC
Article

Synthesis, Structure, Reactivity, and Intramolecular Donor−Acceptor Interactions in a Phosphinoferrocene Stibine and Its Corresponding Phosphine Chalcogenides and Stiboranes

Jiří Schulz, Jakub Antala, David Rezazgui, Ivana Císařová, and Petr Štěpnička*

Cite This: *Inorg. Chem.* 2023, 62, 14028−14043
Read Online

ABSTRACT: Ferrocene-based phosphines equipped with additional functional groups are versatile ligands for coordination chemistry and catalysis. This contribution describes a new compound of this type, combining phosphine and stibine groups at the ferrocene backbone, viz. 1-(diphenylphosphino)-1′-(diphenylstibino)ferrocene (**1**). Phosphinostibine **1** and the corresponding P-chalcogenide derivatives $Ph_2P(E)fcSbPh_2$ (**1E**, fc = ferrocene-1,1′-diyl, E = O, S, Se) were synthesized and further converted to the corresponding stiboranes $Ph_2P(E)fcSb(O_2C_6Cl_4)$-Ph_2 (**6** and **6E**) by oxidation with *o*-chloranil. All compounds were characterized by spectroscopic methods, X-ray diffraction analysis, cyclic voltammetry, and theoretical methods. Both NMR spectroscopy and DFT calculations confirmed the presence of P → Sb and P═O → Sb donor−acceptor interactions in **6** and **6O**, triggered by the oxidation of the stibine moiety into Lewis acidic stiborane. The corresponding interactions in **6S** and **6Se** were of the same type but significantly weaker. A coordination study with AuCl as the model metal fragment revealed that the phosphine group acts as the "primary" coordination site, in line with its higher basicity. The obtained Au(I) complexes were applied as catalysts in the Au-catalyzed cyclization of *N*-propargylbenzamide and in the oxidative [2 + 2 + 1] cyclization of ethynylbenzene with acetonitrile and pyridine *N*-oxides. The catalytic results showed that the stibine complexes had worse catalytic performance than their phosphine counterparts, most likely due to the formation of weaker coordination bonds and hence poorer stabilization of the active metal species. Nevertheless, the stibine moiety could be used to fine-tune the properties of the ligated metal center by changing the oxidation state or substituents at the "remote" Sb atom.

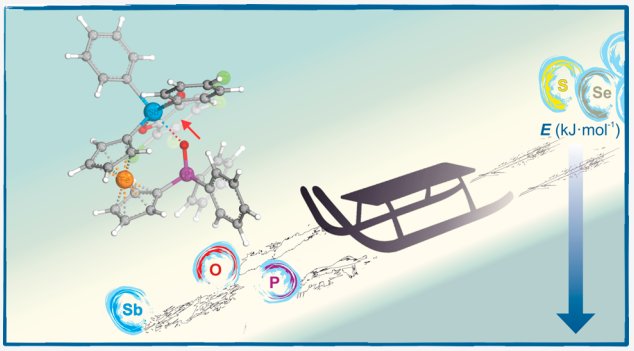

INTRODUCTION

Hybrid ligands[1] possessing distinct donor groups often exhibit coordination behavior and catalytic properties different from those of the corresponding monofunctional derivatives. In particular, phosphinoamine (P,N) ligands, combining the homologous donor moieties, stand out due to their structural versatility, the specific chemical properties and reactivity of the two donor groups, and the possibility of tuning their properties through substituents, resulting in wide catalytic applications.[2,3] A generally similar situation is encountered in the case of phosphinostibine (P,Sb) ligands possessing heavier pnictogen atoms, which have been studied much less thus far. Even in this case, the donor groups significantly differ. Due to an inefficient mixing of the valence s and p orbitals and their more diffuse nature,[4] stibines are worse σ-donors and π-acceptors than phosphines[5] and can even behave as electron density acceptors.[6] The Lewis acidity of stibines can be enhanced by introducing electron-withdrawing substituents and, alternatively, by their oxidation to Sb(V) compounds (stiboranes), which differentiates them from their phosphorus analogues. Compared to the corresponding phosphines, stibines are less sterically demanding due to longer C−Sb bonds and smaller angles between the substituents, which can result in different coordination preferences.[5,7] When combined in one molecule, the phosphine moiety often behaves as the "primary" coordination site, while the stibine group remains uncoordinated or forms additional interactions with Lewis acids or bases.[8,9] Prominent examples of phosphinostibine ligands (Scheme 1) include compounds whose functional groups are connected by methylene or phenylene spacers (**A**[10] and **B**[11]) and the multidonor ligands **C** and **D**.[12,13]

In the chemistry of ferrocene ligands,[14] stibine functional groups have only rarely been used. Until recently, ferrocene stibines were limited mainly to compounds **E** and **F** comprising a 1,2-disubstituted ferrocene backbone, which

Received: June 22, 2023
Published: August 10, 2023

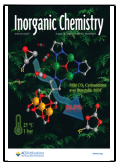

https://doi.org/10.1021/acs.inorgchem.3c02075
Inorg. Chem. 2023, 62, 14028−14043

Scheme 1. Examples of Phosphinostibine Donors (Top, for A–D: R = Various Alkyl and Aryl Groups; X = Cl or R) and Ferrocene Stibines (Bottom, for E: Z = NMe_2, NHR, $NMe_3^+I^-$, OH, OR, SR, etc.; for F: n = 2, 3) Studied to Date and the Structure of 1

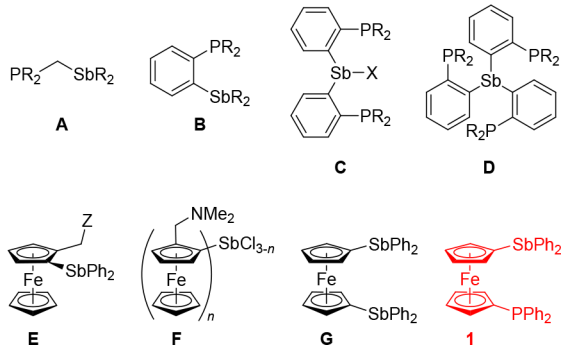

have been studied with a focus on the possible D → Sb interactions (D = adjacent donor moiety; for examples, see Scheme 1).[15] Earlier this year, we reported the synthesis of ferrocene distibine **G** (Scheme 1),[16] a congener of the iconic ferrocene ligand 1,1′-bis(diphenylphosphino)ferrocene (dppf).[17] The facile conversion of this compound into isolable stiboranes and the differences in the reaction behavior of **G** and dppf led us to focus now on the mixed-donor analogue **1**, which represents the missing link between the two symmetrical ligands (Scheme 1). In this contribution, we describe the preparation of this compound and various oxidized derivatives, viz. phosphine-stiborane and phosphine chalcogenide-stiboranes. The resulting compounds are analyzed in view of the difference between the pnictogen donor groups and their possible interactions, which are studied through a combination of experimental and theoretical approaches. Also reported are the results of our preliminary coordination study employing Au(I) as a probe metal ion and the applications of the prepared complexes in gold-catalyzed reactions.

RESULTS AND DISCUSSION

Synthesis of Phosphinostibine 1 and the Corresponding P-Chalcogenides and Stiboranes. Phosphinostibine **1** was prepared by lithiation of 1-bromo-1′-(diphenylphosphino)ferrocene (**2**) with *n*-butyllithium followed by the reaction of the *in situ* generated lithio intermediate with chlorodiphenylstibine (Scheme 2) and was isolated as an air-stable, orange crystalline solid in 76% yield after column chromatography and crystallization. A similar reaction employing 1-bromo-1′-(diphenylphosphino)-ferrocene–borane (1:1) (**1**·BH_3) produced the P-protected phosphinostibine **1**·BH_3, which was smoothly deprotected[18] with 1,4-diazabicyclo[2.2.2]octane (dabco)[19] to give **1**.

Scheme 2. Synthesis of 1 and Its Reaction with MeI

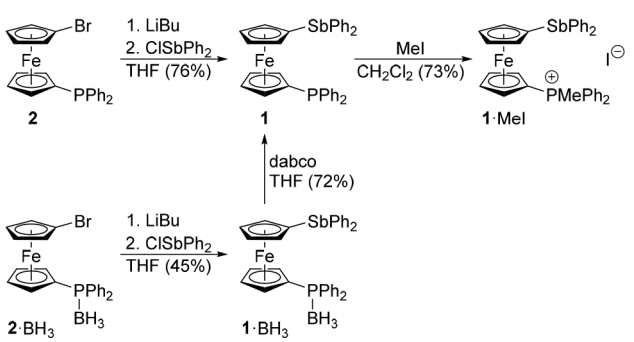

Compounds **1** and **1**·BH_3 were characterized by NMR spectroscopy, ESI MS, and elemental analysis. The ^1H and $^{13}C\{^1H\}$ NMR spectra displayed characteristic signals due to the asymmetrically 1,1′-disubstituted ferrocene units and the phenyl rings, whereas the $^{31}P\{^1H\}$ NMR spectra showed a sharp singlet for **1** (δ_P −16.4; cf. −16.2 for (diphenylphosphino)ferrocene[20]) and a broad doublet-like signal for **1**·BH_3 (δ_P 16.4). Although compound **1** crystallized readily, its structure could not be determined with sufficient precision due to disorder. In the crystal, the P and Sb atoms alternated in their positions with only a minor effect on the overall arrangement, which controlled the crystal packing. Notably, this property was also observed for P-chalcogenides $Ph_2P(E)fcSbPh_2$ (fc = ferrocene-1,1′-diyl) with lighter chalcogen atoms (O and S), which formed shorter P═E bonds (*vide infra*). In contrast, the BH_3 moiety in **1**·BH_3 sufficiently "differentiated" the substituents and, thus, allowed the crystal structure to be determined (Figure 1). The

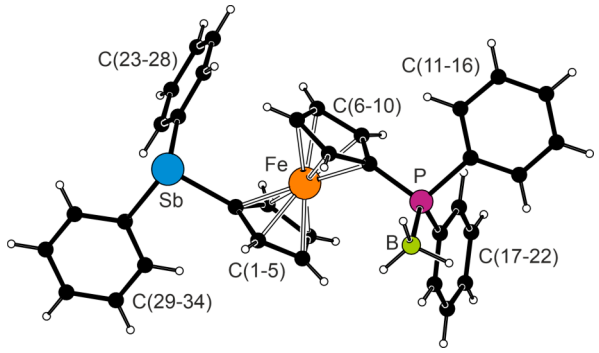

Figure 1. Molecular structure of **1**·BH_3. Selected distances and angles (in Å and deg): Fe–C(1–10) (range) 2.031(3)–2.058(3), Sb–C1 2.131(3), Sb–C23 2.156(3), Sb–C29 2.165(3), C1–Sb–C23 95.6(1), C1–Sb–C29 94.2(1), C23–Sb–C29 96.4(1), P1–B 1.909(4), P–C6 1.789(2), P–C11 1.816(3), P–C17 1.807(3), C6–P–C11 104.5(1), C6–P–C17 107.4(1), C11–P–C17 104.8(1), B–P–C (range) 111.4(1)-114.6(1). A Displacement ellipsoid plot is available in the Supporting Information.

structure of **1**·BH_3 comprises a regular ferrocene unit with parallel cyclopentadienyl rings (dihedral angle 1.5(2)°) and substituents in approximately *anti* positions (the torsion angle τ = C1–Cg1–Cg2–C6, where Cg1 and Cg2 denote the centroids of the cyclopentadienyl rings C(1–5) and C(6–10), respectively, is 160.3(2)°; see Figure S17). The arrangement of the stibine substituent was similar to that in **G**[16] or 1-(diphenylstibino)-2-vinylferrocene,[15b] i.e., with Sb–C(Ph) distances slightly longer than the Sb–C(ferrocenyl) bond and with C(Ph)–Sb–C(Ph) angles wider than the C-(ferrocenyl)–Sb–C(Ph) angles. In turn, the geometry of the phosphine part compared well with that in dppf·2BH_3[21] or 1-(diphenylphosphino)-1-methylferrocene–borane (1:1).[22]

To compare the donor groups present in **1** and to follow their possible interactions, we also prepared the corresponding monofunctional compounds, *viz.* (diphenylphosphino)-ferrocene (**3**) and (diphenylstibino)ferrocene (**4**). The previously unreported stibine **4** was synthesized analogously to **1** (Scheme 3), i.e., by the lithiation of bromoferrocene (**5**) with *n*-butyllithium and subsequent reaction of chlorodiphe-

https://doi.org/10.1021/acs.inorgchem.3c02075
Inorg. Chem. 2023, 62, 14028–14043

Scheme 3. Synthesis of (Diphenylstibino)ferrocene (4)

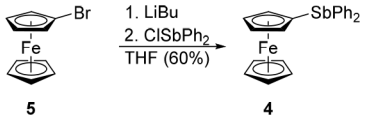

nylstibine. The compound was isolated as an air-stable, orange crystalline solid in 60% yield by crystallization and was fully characterized, including structure determination (Supporting Information; Figure S13).

To quantify the differences between the phosphine and stibine donor groups, we calculated the methyl cation affinities (MCA)[23] of **1**, **3**, and **4** (Table 1). Defined as the enthalpy of

Table 1. Methyl Cation Affinities (MCAs in kJ mol^{-1} at 298.15 K) for 1, 3, and 4[a]

compound	vacuum	chloroform
1 (P)	672	532
1 (Sb)	549	413
3	666	533
4	546	430

[a]Calculated at the PBE0(d3)/def2-TZVP:sdd(Fe,Sb) level of theory. Solvent effects have been approximated using the PCM model. For **1**, the site at which methylation occurred is specified.

$[LB{-}CH_3]^+$ dissociation (LB = Lewis base), larger MCA values are obtained for stronger Lewis bases (LB). In the present case, the MCA values clearly differentiated the pnictogen donor groups in the model compounds, suggesting that the stibine derivative had lower basicity. The presence of the other substituent in the molecule of **1** had only a minor effect on the MCA values estimated for the individual pnictogen substituents (cf. the respective values for **1** and **3**/**4**). The inclusion of solvation phenomena significantly influenced the MCA values, but the general trend remained the same.

These theoretical results corresponded with the outcome of a simple reaction test showing that methylation of **1** with methyl iodide proceeded selectively at the phosphorus atom to afford **1**·MeI in 73% isolated yield (Scheme 2), whereas the stibine group remained intact even when 2 equiv of MeI was used.[24] Selective formation of **1**·MeI was manifested in the NMR spectra, which displayed only one signal attributable to the methyl group, split into a doublet because of interaction with ^{31}P (δ_H 3.05, $^2J_{PH}$ = 13.2 Hz; δ_C 11.64, $^1J_{PC}$ = 60 Hz), while the $^{31}P\{^1H\}$ NMR signal was observed downfield relative to that of the parent compound (δ_P 24.2; cf. 22.6 for **3**·MeI in CD_3CN[25]). An ultimate structure confirmation was provided by X-ray diffraction analysis (see the Supporting Information, Figures S9 and S10). Correspondingly, no borane scrambling between the phosphine and stibine moieties was observed for borane adduct **1**·BH_3 in solution, consistent with the higher basicity of the phosphine group that renders the P−B adduct more stable.[26]

No evidence of a P → Sb donor interaction in **1** was observed. To increase the Lewis acidity of the Sb atom and thus make it amenable for the formation of P → Sb dative interactions, we converted phosphinostibine into phosphinostiborane **6** by oxidation with 3,4,5,6-tetrachloro-1,2-benzoquinone (*o*-chloranil)[27] (Scheme 4). According to the results of the NMR analysis, the reaction of *o*-chloranil (1 equiv) with **1**

Scheme 4. Oxidation of 1 with *o*-Chloranil

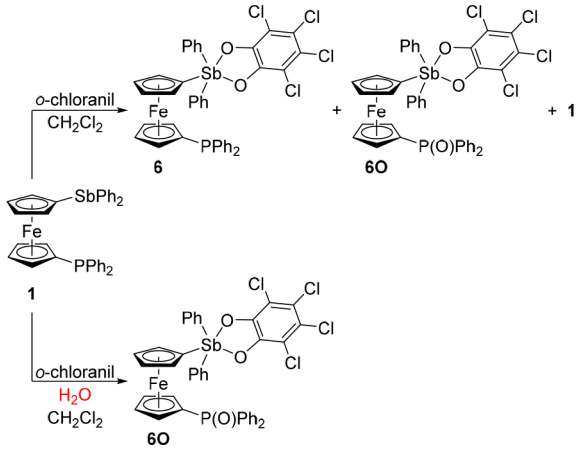

in dichloromethane (1 h/room temperature) produced a mixture of the expected compound **6**, the corresponding phosphine oxide **6O**, and unreacted **1** (ratio of **6**:**6O**:**1** = 28%:35%:37%). The oxidation reaction lacked the selectivity observed in the similar oxidation of 1,2-$Ph_2PC_6H_4SbPh_2$, during which only the stibine moiety was oxidized.[28] Nevertheless, our experiments suggested that the stibine moiety in **1** was oxidized preferentially because the compound $Ph_2P(O_2C_6Cl_4)fcSbPh_2$ with an intact stibine moiety was not detected in the crude reaction mixture. The formation of **6O** can be explained by the 2-fold oxidation of **1** producing $Ph_2P(O_2C_6Cl_4)fcSbPh_2(O_2C_6Cl_4)$ and subsequent (partial) hydrolysis by traces of water.[29] Indeed, performing the reaction under dry conditions but with commercial *o*-chloranil improved the yield of **6** and decreased the amount of hydrolysis product **6O** (**6**:**6O**:**1** = 37%:29%:34%). The components of the reaction mixture were separated by chromatography. Despite the changes in the crude product composition, the isolated yield of **6** remained at approximately 20% due to reactions of this compound with the stationary phase used (silica gel) that resulted in irreversible binding, presumably after hydrolysis of the stiborane moiety. The facile hydrolysis of the presumed doubly oxidized intermediate $Ph_2P(O_2C_6Cl_4)fcSbPh_2(O_2C_6Cl_4)$ was advantageously used to prepare **6O**, which was obtained as the main product upon adding 2 equiv of *o*-chloranil to a dichloromethane solution of **1** containing a few drops of water. Subsequent workup and crystallization afforded **6O** in 65% isolated yield (Scheme 4).

Next, the family of stibine and stiborane derivatives was expanded by compounds featuring heavier P-chalcogenides[30] to establish the possible influence of the chalcogenide donor atom on the E → Sb interaction (Scheme 5). The oxidation changes not only the possible donor atom and the donor···Sb distance but also the electron density distribution in the system. Thus, phosphine oxide **1O** was obtained in two steps from phosphine-bromide **2**, which was oxidized by hydrogen peroxide to **2O** and subsequently lithiated and reacted with $ClSbPh_2$ to produce **1O** (47% yield over the two steps after crystallization; N.B. the direct oxidation of **1** with hydrogen peroxide was not used due to side reactions at the stibine moiety). Phosphine sulfide **1S** and selenide **1Se** were obtained directly by reacting **1** with the corresponding chalcogens in refluxing toluene. The yields were 92% and 83% after crystallization, respectively. Compounds **1S** and **1Se** underwent clean oxidations with *o*-chloranil (1 equiv) to produce **6S**

https://doi.org/10.1021/acs.inorgchem.3c02075
Inorg. Chem. 2023, 62, 14028−14043

Scheme 5. Synthesis of Phosphine Chalcogenides 1E and the Corresponding Stiboranes

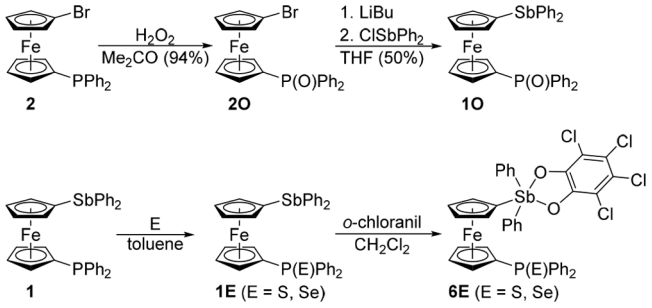

and **6Se**, respectively (~95%; ~5% of **1E** remained unreacted). Despite practically complete conversion, the sulfide was purified by column chromatography and isolated in only 67% yield because it remained partly adsorbed on the silica gel column (most likely after hydrolysis, *vide supra*). Selenide **1Se** could not be purified similarly due to decomposition and adsorption on the column. Alternatively, it was crystallized from hot heptane (66% yield). Increasing the amount of oxidant to 1.1 equiv resulted in complete conversion but also led to decomposition during isolation.

The oxidized phosphine moieties in stibines **1E** (E = O, S, and Se) showed characteristic, downfield-shifted ^{31}P NMR signals (Table 2) and increased J_{PC} coupling constants[31]

Table 2. ^{31}P NMR Shifts (δ_P in ppm) of Compounds 1 and 6[a]

compound	δ_P	compound	δ_P	$\Delta\delta_P$[c]
1	−16.4	**6**	−9.7	+6.7
1O	29.3	**6O**	39.1	+9.8
1S	41.9	**6S**	41.4	−0.5
1Se	32.1 [735][b]	**6Se**	31.8 [726][b]	−0.3

[a]The spectra were recorded in $CDCl_3$ at 25 °C. [b]$^1J_{SeP}$ coupling constant in Hz. [c]Chemical shift difference between **6** and **1**.

compared to **1**. Notably, the chemical shifts were similar to the values reported for chalcogenides derived from **3** (FcP(E)Ph$_2$; E = O, δ_P 30.3,[32] E = S, 41.2 in C_6D_6,[33] and E = Se, 32.7;[20b] Fc = ferrocenyl), which indicated the absence of significant P═E···Sb interactions. The $^1J_{SeP}$ coupling constant determined for **1Se** (735 Hz) was higher than that for FcP(Se)Ph$_2$ (731 Hz),[20b] suggesting a lower basicity of the phosphine group[34] in **1**, which can be ascribed to the presence of an electron-withdrawing stibine substituent that decreased electron density at the ferrocene unit and thus rendered the phosphine less basic.

The structure determination of **1S** and **1Se** ruled out the presence of Sb···E interactions even in the solid state (the structure of **1O** was severely disordered and could not be satisfactorily refined). The sulfide **1S** crystallized as a racemic twin (monoclinic space group *Cc*) with positional disorder of the SbPh$_2$ and P(S)Ph$_2$ moieties, similar to **1** (*vide supra*). No such problems were encountered in the structure of **1Se**. The structures of **1S** and **1Se** were generally similar (Figure 2 and Table 3) with parallel cyclopentadienyl rings and substituents in approximately *anti* positions (see the τ angles in Table 3). A difference was observed in the mutual positioning of the substituents as the Ph$_2$P(S) group was directed with its S atom away from the lone pair at the Sb atom, while the Se atom in

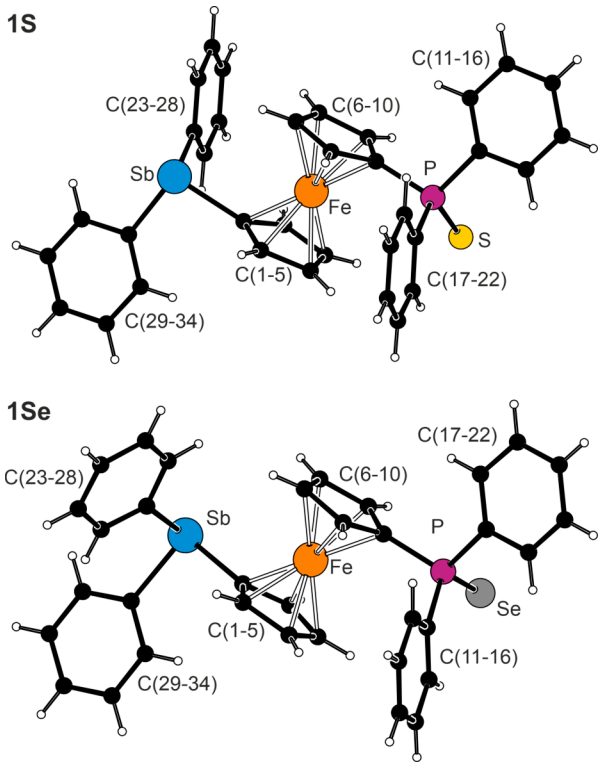

Figure 2. Molecular structures of **1S** and **1Se** (for the sake of clarity, only one position of the disordered substituents in **1S** is shown).

Table 3. Selected Distances and Angles for 1S and 1Se (in Å and deg)

parameter[a]	**1S** (E = S)[c]	**1Se** (E = Se)
Sb−C1	2.125(3)	2.130(2)
Sb−C23/C29	2.160(4)/2.146(4)	2.156(2)/2.165(2)
C−Sb−C[b]	94.9(2)−97.2(2)	94.06(7)−96.74(7)
P═E	1.954(2)	2.1034(7)
P−C6	1.796(4)	1.784(2)
P−C11/C17	1.816(4)/1.806(4)	1.810(2)/1.811(2)
C−P−C[b]	104.9(2)−106.8(2)	104.72(8)−107.25(8)
Fe−C	2.036(4)−2.060(4)	2.034(2)−2.059(2)
tilt	2.0(2)	1.2(1)
τ	169.0(3)	−161.4(1)

[a]Fe−C is the range of the Fe−C(1−10) bond lengths, tilt stands for the dihedral angle of the least-squares cyclopentadienyl planes C(1−5) and C(6−10), and τ denotes the torsion angle C1−Cg1−Cg2−C6, where Cg1 and Cg2 are the centroids of the respective cyclopentadienyl rings. [b]The range of the C1−Sb−C23/29 and C23−Sb−C29 angles. [c]Data for the major orientation.

1Se pointed in the same direction (Figure S17). The parameters of the stibine group were similar to those in **G** and **1**·BH$_3$, while the geometry of the phosphorus substituents compared well with those observed in FcP(S)Ph$_2$,[33] dppfE$_2$,[35] and related compounds.[36]

In contrast, the NMR spectra of stiboranes **6** and **6O** suggested possible P → Sb and P═O → Sb interactions, as the ^{31}P NMR signals shifted downfield relative to those of respective stibines **1** and **1O** (Table 2). For phosphinostiborane **6**, the interaction was further indicated by the splitting of the ^{13}C{^{1}H} NMR signals due to CH and C^{ipso} carbons in the Sb-bound C_5H_4 ring and C^{ipso} of SbPh$_2$ with ^{31}P, while no such coupling was observed for **1**. Conversely, the ^{1}H NMR spectra

https://doi.org/10.1021/acs.inorgchem.3c02075
Inorg. Chem. 2023, 62, 14028−14043

remained virtually unaffected, displaying only signals attributable to a conformationally unconstrained, P^{III}-substituted ferrocene-1,1′-diyl unit, namely, three apparent triplets and one apparent quartet due to the C_5H_4 rings, albeit at a lower field compared to **1** because of the increased electron-withdrawing character of the stiborane substituent (this is consistent with the trend in the redox potentials of ferrocene oxidation, *vide infra*).

In addition, the ^{1}H and $^{13}C\{^{1}H\}$ NMR spectra of **6O** were broadened, suggesting a dynamic structure on the NMR time scale. This was confirmed by a VT ^{1}H NMR study (Figure 3 and Figure S1): the spectrum recorded at −50 °C displayed eight separate signals for the ferrocene CH groups, which became diastereotopic due to a fixed conformation at a low temperature (the ferrocene moiety became axially chiral). Upon increasing the temperature, the signals broadened, and at 25 °C, only three signals were observed for the C_5H_4 protons due to time averaging.

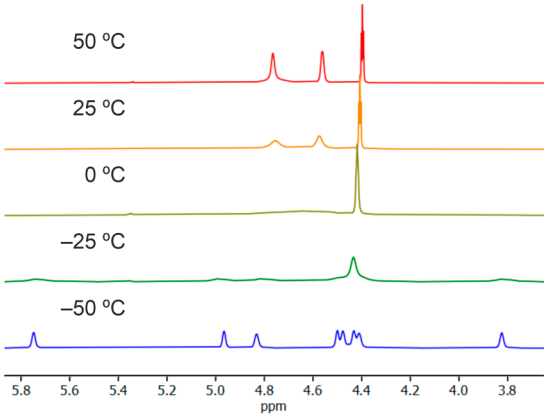

Figure 3. VT ^{1}H NMR spectra (400 MHz, $CDCl_3$) of **6O** showing the region of ferrocene protons (complete spectra are available in the Supporting Information).

Attempts to disrupt the intramolecular P═O → Sb interaction through the addition of competing Lewis bases failed. The NMR spectrum of **6O** remained unchanged upon addition of 4-(dimethylamino)pyridine (1.0 equiv), triethylphosphine oxide (1.3 or 10 equiv), or triphenylphosphine chalcogenides (1.5 equiv; Figure 4 and Figures S2−S4) in $CDCl_3$, and even the spectrum recorded in DMSO-d_6 as a strongly donating solvent suggested that an intramolecular interaction was present. Conversely, the addition of $BF_3{\cdot}OEt_2$ (1 or 5 equiv) as a competing Lewis acid to **6O** cleaved the P═O → Sb dative bond, presumably with concomitant formation of the phosphine oxide−borane adduct $Ph_2P(O)$-$fcSbPh_2(O_2C_6Cl_4){\cdot}BF_3$ (Figure S5). Analogous reaction with $B(C_6F_5)_3$ resulted in decomposition. Similar competing experiments with **6** showed that the intramolecular P → Sb interaction was efficiently canceled by adding 1.5 equiv of Et_3PO, very likely with concomitant formation of **6**·Et_3PO (Figure 4).

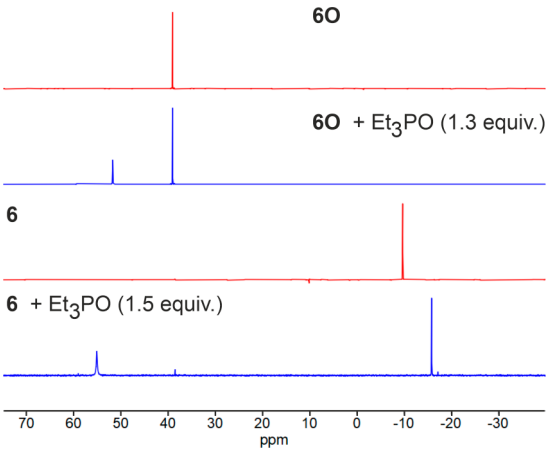

Figure 4. $^{31}P\{^{1}H\}$ NMR spectra (162 MHz, $CDCl_3$, 25 °C) of **6**, **6O**, and their mixtures with Et_3PO.

The intramolecular interactions were clearly detected in the crystal structures of **6**·C_6H_{14} and **6O**·$CHCl_3$ (Figure 5 and Table 4); compounds **6S** and **6Se** did not provide suitable crystals despite numerous attempts. The P → Sb interaction in the molecule of **6** was suggested by the short P···Sb distance (3.0987(6) Å), which is approximately halfway between the sum of the van der Waals radii (3.86 Å)[37] and the sum of the

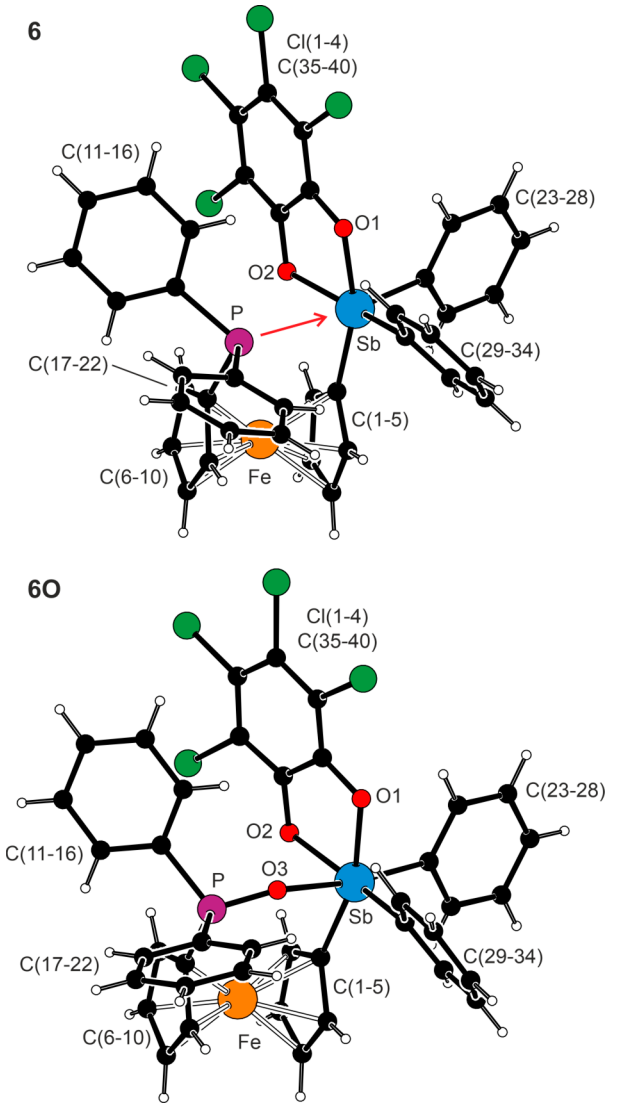

Figure 5. Molecular structures of **6**·C_6H_{14} and **6O**·$CHCl_3$ (the solvent molecules and the less populated orientation of phenyl ring C(17−22) in the molecule of **6** have been omitted for clarity). The P → Sb interaction in molecule **6** is indicated by a red arrow.

https://doi.org/10.1021/acs.inorgchem.3c02075
Inorg. Chem. 2023, 62, 14028−14043

Table 4. Selected Distances and Angles for 6 and 6O·$CHCl_3$ (in Å and deg)

parameter[a]	6·C_6H_{14} (X = P)	6O·$CHCl_3$ (X = O3)[d]
Sb···X	3.0987(6)	2.256(1)
Sb−O1/2	2.068(1)/2.082(1)	2.064(1)/2.076(1)
Sb−C1	2.127(2)	2.116(2)
Sb−C23/C29	2.124(2)/2.138(2)	2.147(2)/2.126(2)
C−Sb−O[b]	161.65(5)/159.94(5)	160.93(6)/162.59(6)
P−C6	1.811(2)	1.779(2)
P−C11/C17	1.839(2)	1.803(2)/1.796(2)
C6−P−C11/C17	101.90(8)/−[c]	107.07(7)/107.07(8)
C11−P−C17	101.3(1)	106.04(8)
Fe−C	2.022(2)−2.057(2)	2.034(2)−2.049(2)
tilt	4.0(1)	2.9(1)
τ	−14.1(1)	5.1(1)

[a]The parameters are defined as for compounds **1S** and **1Se**. See footnote to Table 3. [b]The C1−Sb−O1/C29−Sb−O2 angles for 6·C_6H_{14}, and C29−Sb−O1/C1−Sb−O2 angles for 6O·$CHCl_3$. [c]Value uncertain due to disorder of phenyl ring C(17−22). [d]Further data: P−O3 1.506(1) Å, P−O3−Sb 142.69(7)°.

covalent radii (2.46 Å) of these atoms.[38] Compared to 1·BH_3 containing an intact $SbPh_2$ group, the substituents at the Sb atom were moved apart to provide space for the phosphorus lone pair. For 6·C_6H_{14}, this can be illustrated by wider C−Sb−C angles (∼99−102°) and, mainly, by the τ_5 index of 0.03, which was close to the value expected for an ideal square pyramid (τ_5 = 0; an ideal trigonal bipyramid yields τ_5 = 1).[39] The Sb atom was located 0.28 Å above the {O1, O2, C1, and C29} basal plane, whose minor distortion resulted from the narrower O1−Sb−O2 angle (78.93(5)°) associated with the chelating catecholate ligand (the remaining angles between the basal donor atoms were 86.84(6)−101.95(6)°).

Despite the vicinity of the phosphoryl oxygen atom O3, the geometry around the Sb atom in 6O·$CHCl_3$ remained square pyramidal (τ_5 = 0.03) and was similarly distorted. The Sb atom was displaced by 0.23 Å from the basal plane, and the O3−Sb−C23 angle was nearly linear (172.05(5)°). Even in this case, the Sb···O3 separation (2.256(1) Å) was well below the sum of the van der Waals radii (3.58 Å) but longer than the sum of the covalent radii (2.05 Å). Notably, the O···Sb distance in 6O·$CHCl_3$ was significantly shorter than that in (2-$Ph_2P(O)$-$C_6H_4SbPh_3$)[BF_4] (2.432(2) Å), where the P−O···Sb fragment is bent (∼116°) due to the geometric constraints imposed by the *o*-phenylene backbone.[40] Compared to 6, compound 6O showed shorter P−C bonds and wider C−P−C angles, which is a trend detectable also in the $FcPPh_2$ (3)/$FcP(O)Ph_2$ pair.[41]

Analysis of the Bonding Situation. The nature of the P/P═E → Sb interactions was studied by DFT calculations. Initially, we analyzed the calculated electron densities using the quantum theory of atoms in molecules (QTAIM) approach.[42] The key parameters are summarized in Table 5 and in the Supporting Information (Figure S24).

The Laplacian of the electron density at the bond critical points ($\nabla^2\rho_{bcp}$) between antimony and the donor atom was positive for all stiboranes, indicating some type of closed-shell interaction (ionic, dative, or van der Waals). These weak noncovalent interactions can be distinguished from dative bonds by comparing the relative amounts of potential and kinetic energy at the bond critical point (bcp).[43,44] Specifically, a covalent bonding interaction is indicated by a potential energy density (V_{bcp}, always negative) greater than the kinetic energy density (G_{bcp}, always positive), which yields a negative total energy density ($H = V + G < 0$) or, alternatively, $|V|/G > 1$. The pertinent values indicated that the bonding interactions in stiboranes 6 and 6E were dative bonds (P → Sb or P═E → Sb). Further inspection of the ratios of the kinetic and total energy density to the electron density (ρ_{bcp}), viz. G/ρ_{bcp} and H/ρ_{bcp}, revealed a slightly higher electrostatic contribution for the P═E → Sb interactions (reflected by more positive G/ρ_{bcp} values) than for the P → Sb bond and a comparable degree of covalency (reflected by similarly negative H/ρ_{bcp} values). Both indices were the highest for stiborane 6O, suggesting the strongest interaction in this compound, which corresponds with the experimental results.

This was consistent with the calculated energy difference between the "open" and "closed" forms of stiboranes 6 and 6O (Table 6), which clearly favored the closed form, where the phosphorus groups and stiborane moieties are oriented toward each other and interact (for the structure diagrams, see the Supporting Information, Figure S25). The energy difference, which can be taken as a measure of the strength of the

Table 6. Free Energy Differences (ΔG in kJ mol^{-1} at 298.15 K) between the Open and Closed Isomers of Stiboranes 6, 6O, 6S, and 6Se[a]

compound	vacuum	chloroform
6	−26	−25
6O	−49	−37
6S	−10	−5
6Se	−10	−5

[a]Defined as ΔG = G(closed) − G(open) and calculated at the PBE0(d3)/def2-TZVP:sdd(Fe,Sb) level of theory. Solvent effects have been approximated using the PCM model.

Table 5. Electron Densities (ρ_{bcp}), Laplacians of the Electron Density ($\nabla^2\rho_{bcp}$), Total Electron Densities (H), Ratios of Potential and Kinetic Energy Density ($|V|/G$), and Ratios of Kinetic (G/ρ_{bcp}) and Total Energy Density (H/ρ_{bcp}) to Electron Density at the Bond Critical Point (bcp) Located between the Antimony Atom and a Donor Atom and the Experimental and Calculated Bond Distances

		bond length (Å)							
compd	bond	exp	calc[a]	ρ_{bcp} (e $Å^{-3}$)	$\nabla^2\rho$(r) (e $Å^{-5}$)	H (au)	$\|V\|/G$ (au)	G/ρ_{bcp} (au)	H/ρ_{bcp} (au)
6	P···Sb	3.0987(6)	2.975	0.037	0.028	-0.75×10^{-2}	1.77	0.26	−0.20
6O	O···Sb	2.256(1)	2.293	0.055	0.173	-1.22×10^{-2}	1.44	0.51	−0.22
6S	S···Sb	na[b]	2.915	0.034	0.044	-0.56×10^{-2}	1.48	0.35	−0.17
6Se	Se···Sb	na[b]	2.996	0.034	0.034	-0.62×10^{-2}	1.60	0.30	−0.18

[a]Calculated at the PBE0(d3)/def2-TZVP:sdd(Sb,Fe) level of theory. [b]Not available.

https://doi.org/10.1021/acs.inorgchem.3c02075
Inorg. Chem. 2023, 62, 14028−14043

interaction (N.B. the closed form is expected to be destabilized sterically, which hampers the interaction), in absolute values, decreased from **6O** to **6** to **6S**/**6Se** for isolated species under a vacuum, and the same trend was noted even when considering the solvent effects. However, while the inclusion of solvation phenomena resulted in almost no change in the energy difference for **6**, the values for compounds featuring polar P═E bonds were more affected. In particular, the energy difference for the phosphine oxide **6O** decreased by 12 kJ mol^{-1} upon accounting for the solvation effects, which was attributed to the strong polarization of the P═O bond toward $P^{+}-O^{-}$.[45] Notably, the energy differences determined for **6** and **6O** were significantly higher than the energy barrier for the rotation of the cyclopentadienyl rings in ferrocene itself, which was estimated to be approximately 4 kJ mol^{-1} in the gas phase;[46] those in **6S** and **6Se** were of the same order. The P → Sb interaction in **6** was also manifested by a decreased fluoride ion affinity[47] (305 kJ mol^{-1}) compared to the model compound $FcSbPh_2(O_2C_6Cl_4)$ (341 kJ mol^{-1}), indicating a decreased Lewis acidity of the stiborane moiety in **6** as the result of P → Sb donation.[48]

The presence of dative interactions was further indicated by the calculated Mayer bond orders (MBOs) and Wiberg bond indices (WBIs) (Table 7), which represent the number of electrons shared between two interacting atoms. The lowest values found for stiborane **6O** seemingly did not correspond to the experimental and theoretical results but indicated a more pronounced role for the electrostatic contribution to bonding.

Table 7. Selected Mayer Bond Orders (MBOs) and Wiberg Bond Indices (WBIs) for 6 and 6E[a]

	MBO		WBI	
compound	P/E···Sb	P═E	P/E···Sb	P═E
6	0.49	na	0.22	na
6O	0.13	1.44	0.19	1.92
6S	0.55	1.44	0.21	1.65
6Se	0.57	1.35	0.25	1.49

[a]Calculated at the PBE0(d3)/def2-TZVP:sdd(Fe,Sb) level of theory. na = not applicable.

The dative interactions between the stiborane and phosphine/phosphine-chalcogenide moieties were visualized using intrinsic bond orbital (IBO) analysis.[49] The identified IBOs corroborated the donation of electron density from lone electron pairs located on either the phosphorus or chalcogenide atom to antimony (Figure 6).

The IBO analysis further revealed bonding differences between the phosphine chalcogenide moieties (see the Supporting Information, Figures S26–S28), although the overall description complied well with the generally accepted bonding scheme.[50] The IBO corresponding to the P–O σ-bond in **6O** was largely located at the oxygen atom, confirming the highly polarized nature of this bond. In contrast, the corresponding IBOs in **6S** and **6Se** showed an equal distribution of the bonding electron pairs between the two atoms (phosphorus and chalcogen). Similarly, the π-component of the P–O bond in **6O** differed from those of its heavier congeners, as all three oxygen lone electron pairs were involved in π-interactions with the phosphorus atom, although two of them were involved only to a limited extent. For **6S** and **6Se**, only two electron pairs were involved in the π-bonding interaction, leaving one electron pair essentially nonbonding at the chalcogen atom.[51]

Electrochemistry. The electrochemical behavior of compounds **1** and **6** was studied by cyclic voltammetry on a Pt-disk electrode in dichloromethane by using $Bu_4N[PF_6]$ as the supporting electrolyte. In the accessible range (approximately −1.5 to 2 V vs the ferrocene/ferrocenium reference[52]), compound **1** showed a single redox transition (Figure 7), which was essentially reversible and diffusion-controlled, as indicated by $i_{pa} \propto \nu^{1/2}$ (i_{pa} is the anodic peak current and ν the scan rate; Figures S18 and S19). Such behavior contrasted with the redox response of dppf[53] and analogous compounds,[54] whose electrochemical oxidation was typically associated with follow-up reactions that decreased the reversibility of the electrochemical oxidation. In line with the electron-withdrawing nature of the substituents in **1**, the oxidation occurred 0.14 V more positive than that of ferrocene itself (Table 8) but at a slightly lower potential than the oxidation of dppf under similar conditions ($E^{\circ\prime}$ = 0.17 V vs ferrocene/ferrocenium),[53b] reflecting the lower electronegativity of Sb. The redox responses of **1O** and **1S** were similar, except that the redox

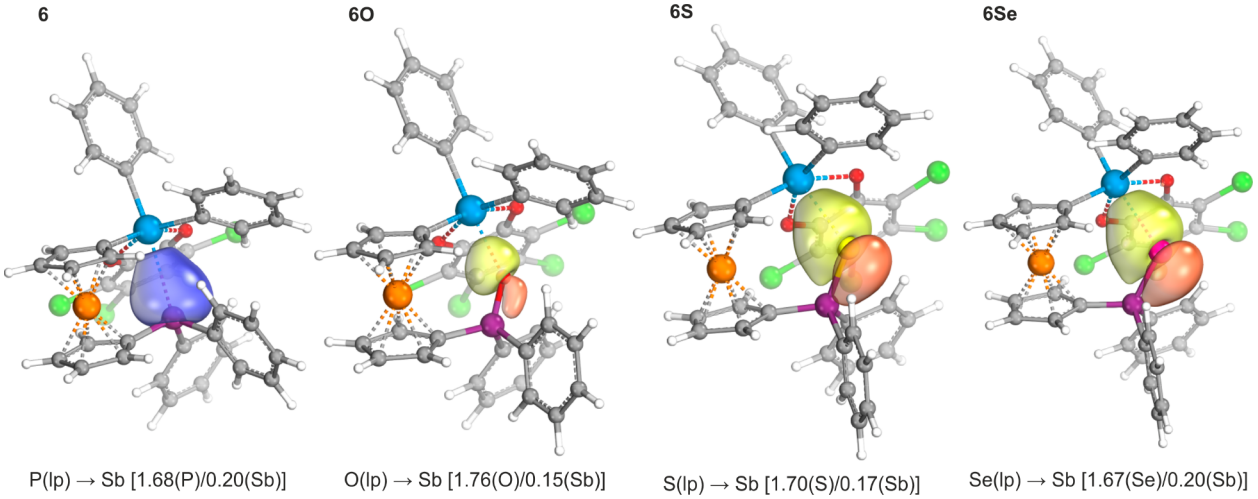

Figure 6. Selected intrinsic bond orbitals (IBOs) of stiboranes **6**, **6O**, **6S**, and **6Se**. Values in parentheses indicate the fraction of bonding electrons assigned to the individual atoms (lp = lone electron pair).

https://doi.org/10.1021/acs.inorgchem.3c02075
Inorg. Chem. 2023, 62, 14028−14043

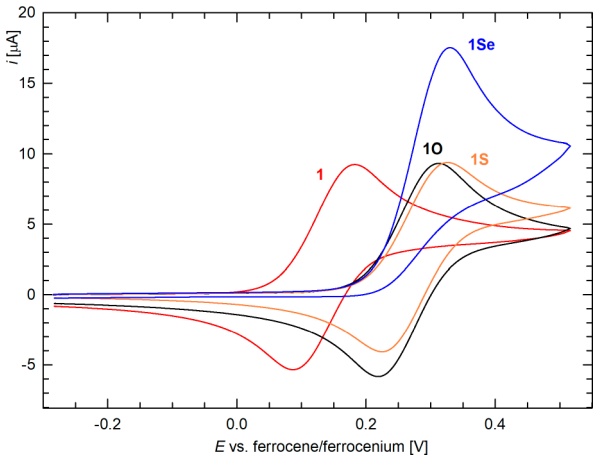

Figure 7. Cyclic voltammograms of **1** and **1E** (Pt-disk electrode, CH_2Cl_2, 0.1 M $Bu_4N[PF_6]$, scan rate 0.1 V s^{-1}).

Table 8. Summary of the Electrochemical Data[a]

compound	$E^{\circ\prime}$ (V)	compound	$E^{\circ\prime}$ (V)
1	0.14	**6**	0.30
1O	0.27	**6O**	0.40
1S	0.29	**6S**	0.42
1Se	0.33[b]	**6Se**	0.48[b]

[a]The measurements were conducted at the Pt-disk electrode in dichloromethane containing 0.1 M $Bu_4N[PF_6]$. The potentials are given in volts relative to ferrocene/ferrocenium references (for details, see the Supporting Information). The potentials for reversible processes were determined as the average of anodic (E_{pa}) and cathodic (E_{pc}) peak potentials, $E^{\circ\prime} = 1/2\ (E_{pa} + E_{pc})$. The separation of the peaks in the cyclic voltammograms was approximately 90 mV due to a large resistance. The decamethylferrocene standard showed similar values. [b]Irreversible wave. The anodic peak potential (E_{pa}) at a scan rate of 100 mV s^{-1} is given.

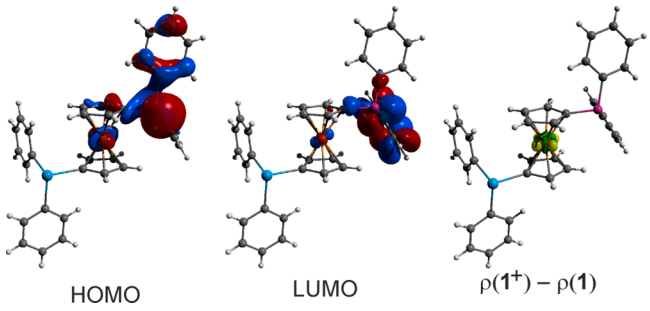

Figure 8. Frontier orbitals (isosurface at ±0.04 au) and the electron difference map $\rho(\mathbf{1}) - \rho(\mathbf{1}^+$ mapped at the geometry of **1**) (isosurface at ±0.02 au) at the PBE0(d3)/def2TZVP level of theory.

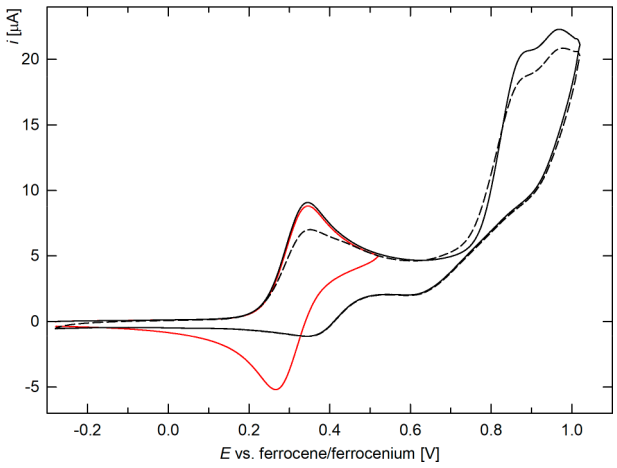

Figure 9. Cyclic voltammograms of **6** (Pt-disk electrode, CH_2Cl_2, 0.1 M $Bu_4N[PF_6]$, scan rate of 0.1 V s^{-1}). The second scan is shown by a dashed line. The peak potentials of the irreversible oxidations are approximately 0.87 and 0.97 V.

waves were shifted toward more positive potentials as a result of the increased electron-withdrawing character of the $P(E)Ph_2$ substituents (Figure 7). The voltammogram of **1S** displayed an additional reductive wave when the scan range was extended toward more positive potentials (Figure S20). Conversely, the oxidation of **1Se** was irreversible and multielectron in nature.[55] At more positive potentials, the selenide underwent another ill-defined oxidation ($E_{pa} \approx 0.89$ V) and showed several weak reductive waves upon a reverse scan (Figure S20).

Based on the results of DFT calculations, the primary oxidation of **1** was assigned to the ferrocene/ferrocenium transition. Although inspection of the frontier orbitals (Figure 8) using natural atomic orbitals (NAOs) showed that the HOMO of **1** corresponds mainly to the lone electron pair of the PPh_2 group, being composed of the phosphorus 3s (~11%) and 3p (~47%) orbitals with a contribution from the 2p orbitals of the proximal carbon atoms (~29%) and the iron 3d orbitals (~5%), a change in the electron density from **1** to $\mathbf{1}^+$, $\rho(\mathbf{1}^+) - \rho(\mathbf{1})$, mapped at the equilibrium geometry of **1**,[56] occurred exclusively at the ferrocene iron, which supported the assignment of the electrochemical oxidation as ferrocene-based. Conversely, the LUMO of **1** was the antibonding combination of carbon 2p orbitals in the π-system of one phenyl ring at the PPh_2 group.

The first oxidation of catecholatostiboranes **6**, **6O**, and **6S** (Figure 9 and Figures S21–S23) was also reversible when they were scanned separately (i.e., when the switching potential was set just after the first redox wave). At higher potentials, however, the compounds displayed several irreversible oxidations, which affected the overall response (e.g., by decreasing the intensity of the first reductive wave and through additional broad reduction features) and resulted in weak reductive waves during the reverse scans. In the case of **6Se**, even the first oxidation was irreversible, and several weak reductive waves were observed, suggesting the instability of the electrochemically generated species. Compared to that of the corresponding stibines, the oxidation of **6** and **6E** was shifted by 0.13–0.16 V toward more positive potentials (Table 8), which indicated a decrease in the electron density at the ferrocene unit upon converting the stibine group into the strongly electron-withdrawing stiboranyl moiety.[57]

Gold Complexes. In view of the intended catalytic testing, the coordination properties of **1** were investigated through reactions with Au(I) precursors. Thus, the reaction of **1** with $[AuCl(SMe_2)]$ at a 1:1 molar ratio in dichloromethane produced the phosphine complex [AuCl(**1**-κP)] (**7**) as the sole product (Scheme 6). When the amount of the gold(I) precursors was increased to 2 equiv, a similar reaction afforded the digold(I) complex $[(\mu(P,Sb)\text{-}\mathbf{1})(AuCl)_2]$ (**8**). Compared to **7**, however, digold complex **8** was *much* less stable, decomposing rapidly in solution and even when stored as a solid at low temperatures in the dark. Attempts to prepare P,Sb-bridged digold complexes via removal of chloride from **7** with $Ag[SbF_6]$ or by the reaction of **1** with $[Au(tht)_2][SbF_6]$

https://doi.org/10.1021/acs.inorgchem.3c02075
Inorg. Chem. 2023, 62, 14028–14043

Scheme 6. Synthesis of AuCl Complexes

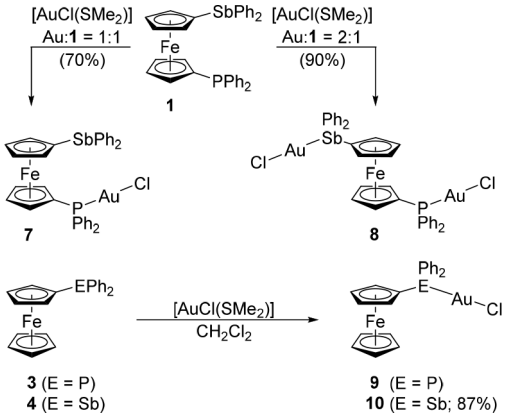

(Au:**1** = 1:1) containing the easily dissociating tetrahydrothiophene ligands (tht) were unsuccessful. Reactions of model compounds **3** and **4** with [AuCl(SMe$_2$)] (1 equiv) produced the respective chlorogold(I) complexes, [AuCl(FcPPh$_2$-κP)] (**9**)[58] and [AuCl(FcSbPh$_2$-κP)] (**10**) (Scheme 6). Even in this pair, the stibine complex was considerably less stable than its phosphine analogue, decomposing in both solution and the solid state.

The coordination of the phosphine moiety was indicated by a downfield shift of the $^{31}P\{^1H\}$ NMR signal (δ_P 28.9 and 27.4 for **7** and **8**, respectively) and changes in the ^1H and $^{13}C\{^1H\}$ NMR spectra (e.g., the $^{13}C\{^1H\}$ NMR signal due to C^{ipso}-P in **7** was shifted to a higher field, and the $^1J_{PC}$ coupling constant increased to 73 Hz from 7 Hz in the free ligand). The coordination of the stibine moiety had no distinct marker (such as the ^{31}P chemical shift) but was indicated by changes in the ^1H and $^{13}C\{^1H\}$ NMR spectra.[59] For **9**, coordination increased the ^1H NMR chemical shifts due to ferrocene protons, and the signal due to ferrocene C^{ipso} shifted upfield (signals due to CH groups experienced smaller changes). The ESI MS of **7** and **8** showed ions due to $[M - Cl]^+$; the spectrum of **10** displayed a major peak due to $[Au(\mathbf{4})_2]^+$ resulting by ligand redistribution and a minor peak of $[M - Cl + Me_2CO]^+$.

Complex **7** reacted cleanly with *o*-chloranil and thionyl chloride to produce stable complexes **11** and **12**, respectively, which were isolated in 78% and 96% yields (Scheme 7). The NMR spectra of these compounds showed the expected signals, including those due to the tetrachlorocatecholate ligand for **11**. The $^{31}P\{^1H\}$ NMR resonances were only marginally affected ($\delta_P \approx 28$), and ESI MS revealed ions attributable to the sodiated species $[M + Na]^+$.

Scheme 7. Oxidation of Complex 7

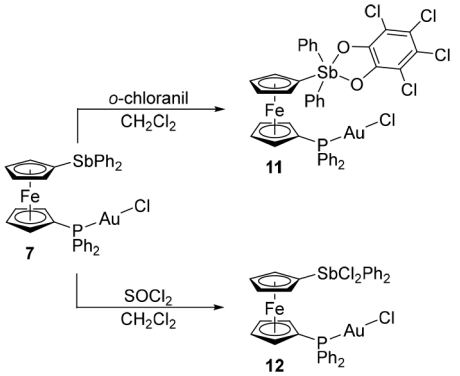

The structures of **7** and **12**·0.4CHCl$_3$ (Figure 10 and Table 9) comprised linear P−Au−Cl moieties (~175°) with Au−P and Au−Cl distances similar to those in [AuCl(PPh$_3$)][60] and **9**.[58] The oxidation changed the geometry at the antimony atom from ψ-tetrahedral to trigonal bipyramidal and shortened the Sb−C bonds (cf. the structures of **G** and the corresponding

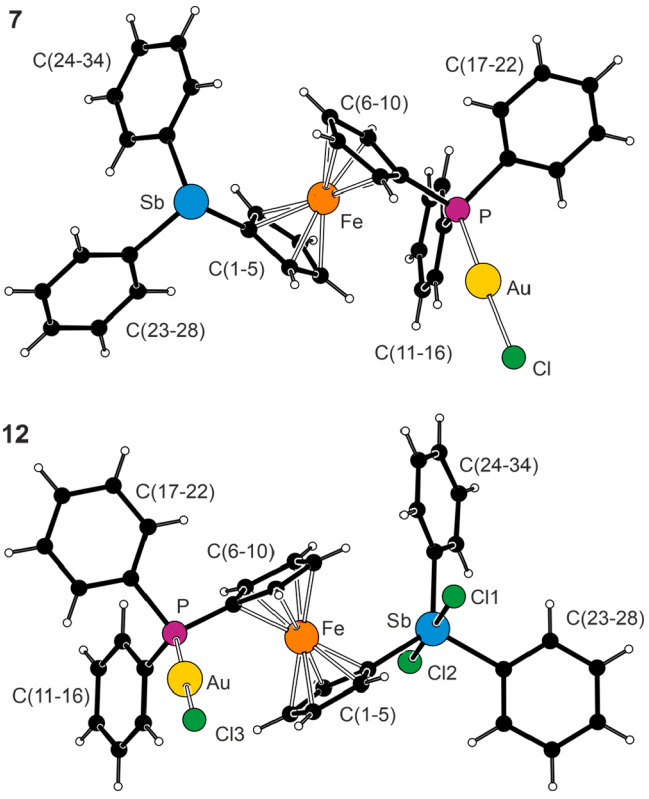

Figure 10. Views of the complex molecules in the structures of **7** and **12**·0.4CHCl$_3$.

Table 9. Selected Distances and Angles for 7 and 12·0.4CHCl$_3$ (in Å and deg)[a]

Parameter	7 (X = void)	12·0.4CHCl$_3$ (X = Cl)[b]
Au−Cl	2.2922(7)	2.2864(7)
Au−P	2.2268(7)	2.2286(6)
P−Au−Cl	174.47(3)	175.34(3)
Sb−X1/2	na	2.4356(6)/2.4875(6)
Sb−C1	2.130(2)	2.096(2)
Sb−C23/C29	2.157(3)/2.152(2)	2.107(2)/2.121(3)
C1−Sb−C23/C29	95.03(9)/95.16(9)	117.08(8)/128.10(9)
C23−Sb−C29	95.95(9)	114.71(9)
P−C6	1.787(2)	1.786(2)
P−C11/C17	1.841(2)/1.818(3)	1.811(2)/1.819(2)
C6−P−C11/17	106.2(1)/103.9(1)	108.1(1)/103.7(1)
C11−P−C17	105.4(1)	103.7(1)
Fe−C	2.028(3)−2.064(3)	2.034(2)−2.062(2)
tilt	2.1(2)	1.1(2)
τ	160.8(2)	174.0(2)

[a]Parameters are defined as for the other compounds discussed in this paper; see the footnote to Table 3. na = not applicable. [b]Further data: Cl−Sb−Cl = 179.49(2)°, Cl−Sb−C (range) = 88.57(6)−91.38(6)°.

https://doi.org/10.1021/acs.inorgchem.3c02075
Inorg. Chem. 2023, 62, 14028−14043

bis(stiborane), [Fe(η^5-$C_5H_4SbPh_2Cl_2)_2$]).[16] The τ_5 parameter for the stiborane moiety in **12** was 0.86, reflecting that although the Cl−Sb−Cl (axial) angle was close to the ideal 180°, the C−Sb−C angles varied (∼115−128°) for steric reasons. The ferrocene units assumed their regular geometry and were negligibly tilted, but the increased steric bulk of the Sb substituent in **12** was reflected by a more open conformation of the ferrocene unit.

The molecular structure of stibine complex **10** (Figure 11) was unexceptional in view of the data determined for **7**, **12**·0.4$CHCl_3$, and [(μ(Sb,Sb)-**G**)$(AuCl)_2$][16] (*vide supra*). The prominent feature that differentiated **10** from the reference compounds was the presence of intermolecular aurophilic interactions[61] between two independent molecules present in the structure (Z' = 2). The Au1···Au2 distance was 2.9992(5) Å, and the interacting P−Au−Cl units were approximately perpendicular to each other (torsion angle Cl1−Au1···Au2−Cl2 was 102.89(4)°). In turn, this suggested that aurophilic interactions can also be responsible for the *multiplication* of the molecules in the asymmetric unit[62] by linking them into supramolecular molecular arrays that behave as the real repeating unit. This hypothesis was verified through a search in the Cambridge Structural Database[63] for structures with intramolecular Au···Au distances in the arbitrary 2.7−3.2 Å range *and* with Z' > 1 (i.e., with two or more formula units *per* asymmetric unit), which resulted in approximately 120 hits (duplicate structures were excluded).[64]

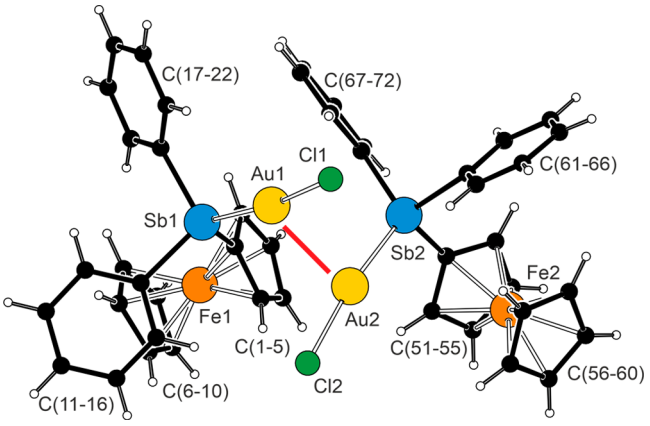

Figure 11. View of the two crystallographically independent molecules of **10**. The Au···Au interaction (Au1···Au2 = 2.9992(5) Å) is indicated by a red line. Selected distances and angles (in Å and deg) for molecule 1 [molecule 2]: Au−Sb 2.4939(4) [2.4945(5)], Au−Cl 2.288(1) [2.3034(9)], Sb−Au−Cl 172.76(3) [169.36(3)].

Catalytic Experiments. Gold(I) complexes **7**, **9**, **10**, and **12**,[65] activated *in situ* with $AgNTf_2$, were applied in Au-mediated cyclization of *N*-propargylbenzamide (**13**) into 4,5-dihydro-5-methylene-2-phenyloxazole (**14**) (Scheme 8).[66] The reactions were performed with 1 mol % of the gold catalyst in CD_2Cl_2 at 25 °C and followed by ^{1}H NMR spectroscopy.[67]

Scheme 8. Gold-Catalyzed Cyclization of *N*-Propargylbenzamide (13) to Oxazole 14

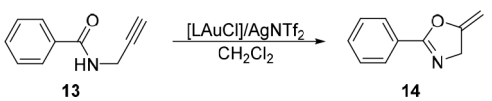

The cyclization reactions proceeded selectively; no other products were detected in the spectra. The kinetic profiles shown in Figure 12 indicate a superior catalytic performance of

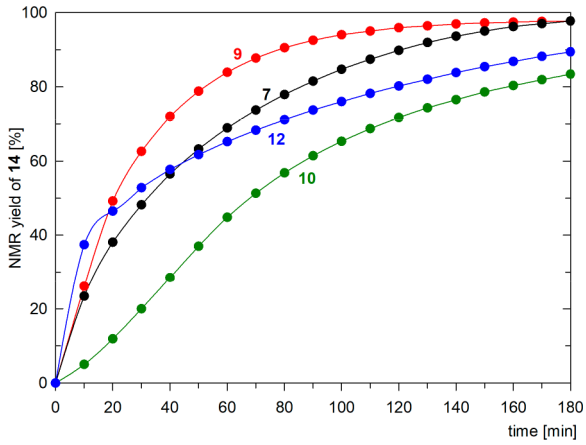

Figure 12. Kinetic profiles for Au-catalyzed cyclization of **13** into oxazole **14** using complexes **7**, **9**, **10**, and **12** as precatalysts. The solid lines are shown only as a guide for an eye.

complex **9** containing phosphine **3**, which maintained a relatively high activity, comparable to the prototypical catalyst [Au(MeCN)(PPh_3)][SbF_6],[67,68] and resulted in a 97% NMR yield after 3 h (complete conversion was achieved after 6 h). The yield of **14** obtained with phosphine complex **7** was similar but was reached at a slower reaction rate. Notably, oxidation of the stibine moiety, such as in **12**, accelerated the reaction at the initial stages (indicated by a visual comparison of the reaction rates during the first 10−20 min of the reaction), but then, the reaction rate decreased, very likely due to catalyst decomposition. The catalyst with the slowest reaction rate was obtained from complex **10**, which presumably reflected the lower stability of this compound and, consequently, easier catalyst decomposition. Nevertheless, the yield of **14** was 82% after a 3 h reaction time. $AgNTf_2$ itself did not catalyze the reaction (N.B.: a further analysis, e.g., an estimation of the initial reaction rates, was not performed, as it could be misleading due to catalyst activation and decomposition).

Next, we investigated the more challenging Au-catalyzed oxidative [2 + 2 + 1] cyclization of ethynylbenzene (**15**) with acetonitrile, used as a solvent, and pyridine *N*-oxides as the oxidants to afford 2-methyl-5-phenyloxazole (**16**; Scheme 9).[69] The initial screening (Table 10, entries 1−8) using catalysts

Scheme 9. Gold-Catalyzed Oxidative [2 + 2 + 1] Annulation of Ethynylbenzene, Acetonitrile, and Pyridine *N*-Oxides

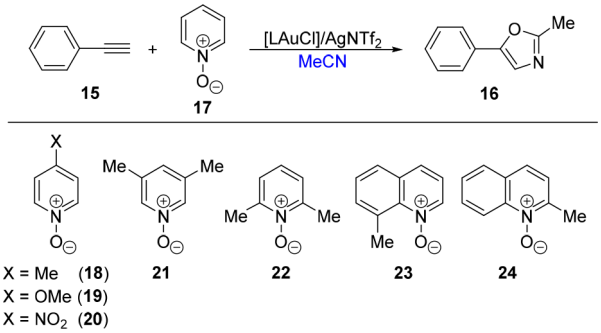

https://doi.org/10.1021/acs.inorgchem.3c02075
Inorg. Chem. 2023, 62, 14028−14043

Table 10. Summary of the Catalytic Results for the Au-Catalyzed Formation of Oxazole 16[a]

entry	Au complex	oxidant	yield of **16** (%)
1	**7**	**17**	37
2	**9**	**17**	51
3	**10**	**17**	0
4	**12**	**17**	27
5[b]	**12**	**17**	4
6	none	**17**	0
7[c]	**12**	**17**	40
8[d]	**12**	**17**	38
9	**7**	**18**	23
10	**7**	**19**	3
11	**7**	**20**	19
12	**7**	**21**	28
13	**7**	**22**	15
14	**7**	**23**	73 (61)[f]
15	**7**	**24**	11
16[e]	**7**	**23**	69 (56)[f]

[a]Conditions unless specified otherwise: alkyne **17** (c = 0.10 M) was added to a mixture of gold complex (5 mol %), $AgNTf_2$ (5 mol %), and oxidant (1.3 equiv) in MeCN at 60 °C for 24 h. The yields were determined by ^1H NMR spectroscopy using anisole (1 equiv) as an internal standard and are an average of two independent runs. [b]No silver salt was used. [c]2 equiv of $AgNTf_2$ was added. [d]3 equiv of $AgNTf_2$ was added. [e]$Ag[SbF_6]$ was used instead of $AgNTf_2$. [f]Isolated yield in parentheses.

generated *in situ* from the defined Au(I) complexes (5 mol %), $AgNTf_2$ (1 equiv), and pyridine *N*-oxide (**17**), performed at 60 °C for 24 h, showed that only phosphine complexes efficiently mediated this reaction. The yields of **16** achieved with complexes **7** and **9** were 37% and 51%, respectively. A lower yield, 27%, was obtained with compound **12**, whereas no appreciable reaction was observed when the stibine complex **10** was used as the precatalyst. Subsequent experiments focused on complex **7** showed that this compound alone (i.e., without the silver(I) salt) was also active but resulted in a significantly lower yield (4%). Adding 2 or 3 equiv of $AgNTf_2$ to complex **12** improved the yield of the cyclization product to approximately 40%.

Since the outcome of this catalytic reaction[69] is known to depend on the *N*-oxide component, we screened several *N*-oxides (Table 10, entries 9−15). The yields achieved with substituted pyridine *N*-oxides **18**-**22** were substantially lower than those achieved with the parent compound **17**, irrespective of the electronic properties of the substituents and steric bulk. An improvement to a 73% yield of **16** was observed when using the sterically encumbered 8-methylquinoline *N*-oxide (**23**), while the reaction in the presence of the isomeric 2-methylquinoline *N*-oxide (**24**) gave only an 11% yield. When $AgNTf_2$ was replaced with $Ag[SbF_6]$ in the reaction with **7** and the best-performing oxidant **23**, the yield of the cyclization product decreased slightly (to 68%), very likely for solubility reasons ($AgNTf_2$ is more soluble in organic solvents).

CONCLUSION

Reported here are the synthesis, detailed structural characterization, and reactivity studies of 1-(diphenyphosphino)-1′-(diphenylstibino)ferrocene (**1**), which is the first ferrocene-based phosphinostibine ligand, falling halfway between the widely studied 1,1′-bis(diphenylphosphino)ferrocene (dppf)[17] and 1,1′-bis(diphenylstibino)ferrocene (**G**) reported only recently.[16] Although compounds combining phosphine and stibine donor groups are not unprecedented, phosphinostibine **1** is unique thanks to the particular combination of steric and electronic properties of its central ferrocene backbone.[14f,70] As a strong electron donor, the ferrocene moiety increases the electron density at the Sb atom and, thus, decreases its acceptor properties. In addition, the ferrocene scaffold allows mutual reorientation of the functional pnictogen groups attached in positions 1 and 1′ by acting as molecular ball bearing with only low energy barrier. This markedly differentiates compounds **1**, **1E**, **6**, and **6E** (E = O, S, Se) from the previously reported compounds, wherein the P and Sb substituents were typically brought into close proximity by a rigid backbone. Importantly, the functional substituents at the ferrocene unit can be manipulated independently, which allowed the selective synthesis of P(III)/Sb(V), P(V)/Sb(III), and P(V)/Sb(V) derivatives, which were subsequently investigated for possible interactions between the pnictogen groups. While stibines **1** and **1E** virtually lacked donor−acceptor interactions, the more Lewis acidic stiboranes **6** and **6O**, obtained by oxidation of **1** with *o*-chloranil, formed distinct intramolecular interactions of the P → Sb(V) and P═O → Sb(V) type, which were manifested in both the crystal structures and the spectroscopic properties. In contrast, the analogous P═S → Sb(V) and P═Se → Sb(V) interactions in phosphine chalcogenide-stiboranes **6S** and **6Se** were weaker and did not result in the significant stabilization of a particular conformation. DFT calculations were used to investigate the nature of these interactions, and the results showed lone pair donation from phosphine phosphorus (in **6**) or phosphoryl oxygen (in **6O**) to the stiborane Sb atom at the other cyclopentadienyl ring. Although similar in nature, these interactions differed in strength and electrostatic contribution, with that in **6O** being stronger and more ionic due to the strong polarization of the P═O bond.

From another viewpoint, compound **1** can be considered a typical example of a hybrid and potentially hemilabile ligand that forms coordination bonds of different strengths. This is reflected in the stability of the coordination compounds obtained from this ligand and affects the catalytic properties of the obtained complexes. The data collected for complexes containing the soft Au(I) metal ion suggest that stibine coordination does not sufficiently stabilize the active metal species, which is thus prone to decomposition. In turn, this leads to a shorter catalyst lifetime and poorer catalytic performance. A similar observation was previously made for the analogous Pd complexes featuring dppf and **G** as the ligands, among which the phosphine complexes showed better catalytic properties in Suzuki−Miyaura cross-coupling.[16] From this perspective, compound **1** should be considered a functional phosphine whose P atom acts as the primary coordination site for soft metal ions, while the Sb moiety can be used as a secondary donor moiety or a reactive group whose chemical transformations can be used to control the overall electronic properties and an ability to form structure-directing intra- and intermolecular secondary interactions in the complexes.

ASSOCIATED CONTENT

Supporting Information

The Supporting Information is available free of charge at https://pubs.acs.org/doi/10.1021/acs.inorgchem.3c02075.

https://doi.org/10.1021/acs.inorgchem.3c02075
Inorg. Chem. 2023, 62, 14028−14043

Complete experimental and characterization data for the prepared compounds, a summary of crystallographic parameters, additional structure diagrams, and copies of the NMR spectra (PDF)

Coordinate files for the DFT-optimized structures (XYZ)

Accession Codes

CCDC 2268692−2268701 contain the supplementary crystallographic data for this paper. These data can be obtained free of charge via www.ccdc.cam.ac.uk/data_request/cif, or by emailing data_request@ccdc.cam.ac.uk, or by contacting The Cambridge Crystallographic Data Centre, 12 Union Road, Cambridge CB2 1EZ, UK; fax: +44 1223 336033.

AUTHOR INFORMATION

Corresponding Author

Petr Štěpnička − *Department of Inorganic Chemistry, Faculty of Science, Charles University, 128 40 Prague, Czech Republic*; Email: stepnic@natur.cuni.cz

Authors

Jiří Schulz − *Department of Inorganic Chemistry, Faculty of Science, Charles University, 128 40 Prague, Czech Republic*

Jakub Antala − *Department of Inorganic Chemistry, Faculty of Science, Charles University, 128 40 Prague, Czech Republic*

David Rezazgui − *Department of Inorganic Chemistry, Faculty of Science, Charles University, 128 40 Prague, Czech Republic*

Ivana Císařová − *Department of Inorganic Chemistry, Faculty of Science, Charles University, 128 40 Prague, Czech Republic*

Complete contact information is available at: https://pubs.acs.org/10.1021/acs.inorgchem.3c02075

Author Contributions

The manuscript was written through the contributions of all authors. All authors have approved the final version of the manuscript.

Notes

The authors declare no competing financial interest.

ACKNOWLEDGMENTS

This work was supported by the Czech Science Foundation (project no. 21-02316S). Computational resources were provided by the e-INFRA CZ project (ID: 90254), supported by the Ministry of Education, Youth and Sports of the Czech Republic.

REFERENCES

(1) Jeffrey, J. C.; Rauchfuss, T. B. Metal Complexes of Hemilabile Ligands. Reactivity and Structure of Dichlorobis(*o*-(diphenylphosphino)anisole)ruthenium(II). *Inorg. Chem.* **1979**, *18*, 2658−2666.

(2) (b) Braunstein, P.; Naud, F. Hemilability of Hybrid Ligands and the Coordination Chemistry of Oxazoline-Based Systems. *Angew. Chem., Int. Ed.* **2001**, *40*, 680−699. (a) Slone, C. S.; Weinberger, D. A.; Mirkin, C. A.; Karlin, K. D. The Transition Metal Coordination Chemistry of Hemilabile Ligands. *Prog. Inorg. Chem.* **2007**, 233−350.

(3) For an overview of the chemistry of ferrocene-based P,N-ligands, see: Dwadnia, N.; Roger, J.; Pirio, N.; Cattey, H.; Hierso, J.-C. Input of P, N-(phosphanyl, amino)-ferrocene hybrid derivatives in late transition metals catalysis. *Coord. Chem. Rev.* **2018**, *355*, 74−100. See also ref 12.

(4) Kutzelnigg, W. Chemical Bonding in Higher Main Group Elements. *Angew. Chem., Int. Ed.* **1984**, *23*, 272−295.

(5) (a) Champness, N. R.; Levason, W. Coordination chemistry of stibine and bismuthine ligands. *Coord. Chem. Rev.* **1994**, *133*, 115−217. (b) Werner, H. The Way into the Bridge: A New Bonding Mode of Tertiary Phosphanes, Arsanes and Stibanes. *Angew. Chem., Int. Ed.* **2004**, *43*, 938−954. (c) Levason, W.; Reid, G. Developments in the coordination chemistry of stibine ligands. *Coord. Chem. Rev.* **2006**, *250*, 2565−2594. (d) Greenacre, V. K.; Levason, W.; Reid, G. Developments in the chemistry of stibine and bismuthine complexes. *Coord. Chem. Rev.* **2021**, *432*, 213698. (e) Lipshultz, J. M.; Li, G.; Radosevich, A. T. Main Group Redox Catalysis of Organopnictogens: Vertical Periodic Table Trends and Emerging Opportunities in Group 15. *J. Am. Chem. Soc.* **2021**, *143*, 1699−1721. (f) Hollingsworth, W. M.; Hill, E. A. Exploring the potential role of heavy pnictogen elements in ligand design for new metal-ligand cooperative chemistry. *J. Coord. Chem.* **2022**, *75*, 1436−1466.

(6) Benjamin, S. L.; Reid, G. Neutral organoantimony(III) and organobismuth(III) ligands as acceptors in transition metal complexes − Role of substituents and co-ligands. *Coord. Chem. Rev.* **2015**, *297*−*298*, 168−180.

(7) For recent examples, see: (a) Benjamin, S. L.; Krämer, T.; Levason, W.; Light, M. E.; Macgregor, S. A.; Reid, G. [$Pd_4(\mu_3$-$SbMe_3)_4(SbMe_3)_4$]: A Pd(0) Tetrahedron with μ_3-Bridging Trimethylantimony Ligands. *J. Am. Chem. Soc.* **2016**, *138*, 6964−6967. (b) Jolleys, A.; Lake, B. R. M.; Krämer, T.; Benjamin, S. L. A Five-Membered $PdSb_n$ Coordination Series. *Organometallics* **2018**, *37*, 3854−3862. (c) Benjamin, S. L.; Levason, W.; Reid, G.; Warr, R. P. Halostibines $SbMeX_2$ and $SbMe_2X$: Lewis Acids or Lewis Bases? *Organometallics* **2012**, *31*, 1025−1034.

(8) The affinity of Lewis acidic stibine and stiborane groups toward Lewis bases was exploited to design ion sensors. For representative examples, see: (a) Wade, C. R.; Ke, I.-S.; Gabbaï, F. P. Sensing of Aqueous Fluoride Anions by Cationic Stibine-Palladium Complexes. *Angew. Chem., Int. Ed.* **2012**, *51*, 478−481. (b) Hirai, M.; Gabbaï, F. P. Lewis acidic stiborafluorenes for the fluorescence turn-on sensing of fluoride in drinking water at ppm concentrations. *Chem. Sci.* **2014**, *5*, 1886−1893. (c) Christianson, A. M.; Gabbaï, F. P. A Lewis Acidic, π-Conjugated Stibaindole with a Colorimetric Response to Anion Binding at Sb(III). *Organometallics* **2017**, *36*, 3013−3015.

(9) For other examples, see: (a) Rat, C. I.; Silvestru, C.; Breunig, H. J. Hypervalent organoantimony and -bismuth compounds with pendant arm ligands. *Coord. Chem. Rev.* **2013**, *257*, 818−879. (b) Benjamin, S. L.; Levason, W.; Reid, G.; Rogers, M. C. Hybrid dibismuthines and distibines as ligands towards transition metal carbonyls. *Dalton Trans.* **2011**, *40*, 6565−6574. (c) Benjamin, S. L.; Karagiannidis, L.; Levason, W.; Reid, G.; Rogers, M. C. Hybrid Dibismuthines and Distibines: Preparation and Properties of Antimony and Bismuth Oxygen, Sulfur, and Nitrogen Donor Ligands. *Organometallics* **2011**, *30*, 895−904.

(10) (a) Kauffmann, T.; Joußen, R.; Klas, N.; Vahrenhorst, A. Neue Reagenzien, XXV. [(Diphenylstibino)methyl]lithium und -kupfer(I); Synthese und präparative Anwendungen. *Chem. Ber.* **1983**, *116*, 473−478. (b) Manger, M.; Wolf, J.; Laubender, M.; Teichert, M.; Stalke, D.; Werner, H. The First Peralkylated Phosphino(stibino)methanes and Their Organometallic Rhodium Complexes. *Chem. Eur. J.* **1997**, *3*, 1442−1450. (c) Manger, M.; Gevert, O.; Werner, H. Unusual Dinuclear Hydridorhodium(III) Complexes Containing Bulky Phosphinyl(stibanyl)methanes as Chelating Ligands. *Chem. Ber.* **1997**, *130*, 1529−1531. For the synthesis of $Sb(CH_2PPh_2)_3$, see: (d) Karsch, H. H.; Witt, E. Phosphinomethanides and Group 15 element halides: Redox reactions, rearrangements and novel heterocycles. *J. Organomet. Chem.* **1997**, *529*, 151−169.

(11) Selected examples: (a) Levason, W.; McAuliffe, C. A. Bidentate ligands containing very soft donor atoms. Nickel(II) complexes of arylarsines and arylstibines. *Inorg. Chim. Acta* **1974**, *11*, 33−40. (b) Levason, W.; McAuliffe, C. A. Bidentate Group VB ligands. Part XVII. Palladium(II), platinum(II), and rhodium(III) complexes of *o*-phenylenebis(diphenylphosphine), (*o*-diphenylphosphinophenyl)-

diphenylstibine, and (*o*-diphenylarsinophenyl)diphenylstibine. *Inorg. Chim. Acta* **1976**, *16*, 167−172. (c) Levason, W.; Smith, K. G.; McAuliffe, C. A.; McCullough, F. P.; Sedgwick, R. D.; Murray, S. G. Synthesis and properties of group 5B ligand analogues of *o*-phenylenebis(dimethylarsine), *o*-$C_6H_4(EMe_2)(E'Me_2)$ where E, E′ = P, N, As, or Sb. *J. Chem. Soc., Dalton Trans.* **1979**, 1718−1724. (d) Talay, R.; Rehder, D. Carbonylvanadium, -manganese and -molybdenum complexes of the ligands *o*-$C_6H_4EPh_2(E'Ph_2)$ (E,E′ = P, As, Sb, Bi) and *cis*-$Ph_2PCH = CHPPh_2$. *Z. Naturforsch.* **1981**, *36b*, 451−462. (e) Gray, L. R.; Hale, A. L.; Levason, W.; McCullough, F. P.; Webster, M. Diphosphine and diarsine complexes of chromium(III). Crystal and molecular structure of tetra-*n*-propylammonium [*cis*-1,2-bis(diphenylphosphino)ethene]tetrachlorochromate(III). *J. Chem. Soc., Dalton Trans.* **1983**, 2573−2580. (f) Black, J. R.; Levason, W.; Spicer, M. D.; Webster, M. Synthesis and solution multinuclear magnetic resonance studies of homoleptic copper(I) complexes of Group 15 donor ligands. *J. Chem. Soc.; Dalton Trans.* **1993**, 3129−3136. (g) Jewiss, H. C.; Levason, W.; Spicer, M. D.; Webster, M. Coordination chemistry of higher oxidation states. 25. Synthesis and properties (including ^{59}Co NMR Spectra) of cobalt(III) complexes of ligands containing two tertiary stibine groups. Crystal structure of *trans*-$[Co\{o\text{-}C_6H_4(SbMe_2)_2\}_2Cl_2]_2[CoCl_4]$. *Inorg. Chem.* **1987**, *26*, 2102−2016. (h) Chalmers, B. A.; Bühl, M.; Arachige, K. S. A.; Slawin, A. M. Z.; Kilian, P. Structural, Spectroscopic and Computational Examination of the Dative Interaction in Constrained Phosphine-Stibines and Phosphine-Stiboranes. *Chem. Eur. J.* **2015**, *21*, 7520−7531. (i) Chalmers, B. A.; Meigh, C. B. E.; Nejman, P. S.; Bühl, M.; Lébl, T.; Woollins, J. D.; Slawin, A. M. Z.; Kilian, P. Geminally Substituted Tris(acenaphthyl) and Bis(acenaphthyl) Arsines, Stibines, and Bismuthine: A Structural and Nuclear Magnetic Resonance Investigation. *Inorg. Chem.* **2016**, *55*, 7117−7125. (j) Jones, J. S.; Gabbaï, F. P. Activation of an Au−Cl Bond by a Pendent Sb^{III} Lewis Acid: Impact on Structure and Catalytic Activity. *Chem. Eur. J.* **2017**, *23*, 1136−1144. For a binaphthyl derivative, see: (k) Yasuike, S.; Kawara, S.; Okajima, S.; Seki, H.; Yamaguchi, K.; Kurita, J. Non-C_2-symmetrical antimony−phosphorus ligand, (*R*/*S*)-2-diphenylphosphano-2′-di(p-tolyl)stibano-1,1′-binaphthyl (BINAPSb): preparation and its use for asymmetric reactions as a chiral auxiliary. *Tetrahedron Lett.* **2004**, *45*, 9135−9138.

(12) (a) Dawson, J. W.; Venanzi, L. M. Phosphorus-31 nuclear magnetic resonance studies of coordination compounds. I. Stereochemistry of some complexes with multidentate ligands. *J. Am. Chem. Soc.* **1968**, *90*, 7229−7233. (b) Higginson, B. R.; McAuliffe, C. A.; Venanzi, L. M. Anomalous ligand field effects in complexes of quadridentate ligands containing Group V donors. *Inorg. Chim. Acta* **1971**, *5*, 37−40. (c) Wade, C. R.; Gabbaï, F. P. Two-Electron Redox Chemistry and Reversible Umpolung of a Gold−Antimony Bond,. *Angew. Chem., Int. Ed.* **2011**, *50*, 7369−7372. (d) Ke, I.-S.; Gabbaï, F. P. *σ*-Donor/Acceptor-Confused Ligands: The Case of a Chlorostibine. *Inorg. Chem.* **2013**, *52*, 7145−7151. (e) Ke, I.-S.; Gabbaï, F. P. $Cu_3(\mu_2\text{-}Cl)_3$ and $Ag_3(\mu_2\text{-}Cl)_3$ Complexes Supported by Tetradentate Trisphosphino-stibine and -bismuthine Ligands: Structural Evidence for Triply Bridging Heavy Pnictines. *Aust. J. Chem.* **2013**, *66*, 1281−1287. (f) Jones, J. S.; Wade, C. R.; Gabbaï, F. P. Redox and Anion Exchange Chemistry of a Stibine-Nickel Complex: Writing L, X, Z Ligand Alphabet with a Single Element. *Angew. Chem., Int. Ed.* **2014**, *53*, 8876−8879. (g) Ke, I.-S.; Jones, J. S.; Gabbaï, F. P. Anion-Controlled Switching of an X Ligand into a Z Ligand: Coordination Non-innocence of a Stiboranyl Ligand. *Angew. Chem., Int. Ed.* **2014**, *53*, 2633−2637. (h) Yang, H.; Gabbaï, F. P. Activation of an Hydroamination Gold Catalyst by Oxidation of a Redox-Noninnocent Chlorostibine Z-Ligand. *J. Am. Chem. Soc.* **2015**, *137*, 13425−13432. (i) You, D.; Gabbaï, F. P. Unmasking the Catalytic Activity of a Platinum Complex with a Lewis Acidic, Non-innocent Antimony Ligand. *J. Am. Chem. Soc.* **2017**, *139*, 6843−6846. (j) Jones, J. S.; Wade, C. R.; Yang, M.; Gabbaï, F. P. On the coordination non-innocence of antimony in nickel(II) complexes of the tetradentate (*o*-$(Ph_2PC_6H_4)_3Sb$ ligand. *Dalton Trans.* **2017**, *46*, 5598−5604. (k) Sen, S.; Ke, I.-S.; Gabbaï, F. P. T-Shaped Gold→Stiborane Complexes as Carbophilic Catalysts: Influence of the Peripheral Substituents. *Organometallics* **2017**, *36*, 4224−4230. (l) Piesch, M.; Gabbaï, F. P.; Scheer, M. Phosphino-Stibine Ligands for the Synthesis of Heterometallic Comlexes. *Z. Anorg. Allg. Chem.* **2021**, *647*, 266−278. For similar ligands with acenaphthene scaffold, see: (m) Furan, S.; Hupf, E.; Boidol, J.; Brünig, J.; Lork, E.; Mebs, S.; Beckmann, J. Transition metal complexes of antimony centered ligands based upon acenaphthyl scaffolds. Coordination non-innocent or not? *Dalton Trans.* **2019**, *48*, 4504−4513.

(13) For a recent example of Sb,N- and Bi,N-ligands, see: Garcia-Romero, A.; Waters, J. E.; Jethwa, R. B.; Bond, A. D.; Colebatch, A. L.; Garcia-Rodriguez, R.; Wright, D. S. Highly Adaptive Nature of Group 15 *Tris*(quinolinyl) Ligands−Studies with Coinage Metals. *Inorg. Chem.* **2023**, *62*, 4625−4636.

(14) (a) *Ferrocenes. Homogeneous Catalysis. Organic Synthesis. Materials Science*; Togni, A., Hayashi, T.; Eds.; VCH: 1995. (b) Atkinson, R. C. J.; Gibson, V. C.; Long, N. J. The syntheses and catalytic applications of unsymmetrical ferrocene ligands. *Chem. Soc. Rev.* **2004**, *33*, 313−328. (c) Gomez Arrayas, R.; Adrio, J.; Carretero, J. C. Recent Applications of Chiral Ferrocene Ligands in Asymmetric Catalysis. *Angew. Chem., Int. Ed.* **2006**, *45*, 7674−7715. (d) *Ferrocenes: Ligands, Materials and Biomolecules*, Štěpnička, P.; Ed.; Wiley: 2008. (e) Cunningham, L.; Benson, A.; Guiry, P. J. Recent developments in the synthesis and applications of chiral ferrocene ligands and organocatalysts in asymmetric catalysis. *Org. Biomol. Chem.* **2020**, *18*, 9329−9370. (f) Štěpnička, P. Forever young: the first seventy years of ferrocene. *Dalton Trans.* **2022**, *51*, 8085−8102.

(15) (a) Sharma, P.; Lopez, J. G.; Ortega, C.; Rosas, N.; Cabrera, A.; Alvarez, C.; Toscano, A.; Reyes, E. First ferrocenylstibines and their molecular structures. *Inorg. Chem. Commun.* **2006**, *9*, 82−85. (b) Vázquez, J.; Sharma, P.; Cabrera, A.; Toscano, A.; Hernández, S.; Pérez, J.; Gutiérrez, R. Formation of (vinyl-ferrocenyl)stibines involving *β*-elimination: Hypervalent Sb−N bonding. *J. Organomet. Chem.* **2007**, *692*, 3486−3491. (c) Ortiz, A. M.; Sharma, P.; Pérez, D.; Rosas, N.; Velasco, L.; Toscano, A.; Hernández, S. New 1,2-disubstituted ferrocenyl stibines containing N-heterocyclic pendant arm: Sb−N hypervalent compounds. *J. Organomet. Chem.* **2009**, *694*, 2037−2042. (d) Pérez, D.; Sharma, P.; Cabrera, A.; Rosas, N.; Arellano, I.; Toscano, A.; Hernández, S. Preparation of new 1,2-disubstituted ferrocenyl stibines containing ether/thioether arm from a quaternarny ferrocenyl ammonium salt. *Polyhedron* **2009**, *28*, 3115−3119. For 1,1′-ferrocene derivatives, see: (e) Perez, D.; Herrera, C.; Sharma, M.; Gutierrez, R.; Hernández, S.; Toscano, A.; Sharma, P. Synthesis of C_3-symmetric *tris*(1,1′-formylferrocenyl)stibine and bismuthine: Rare examplex of *tris* 1,1′-asymmetrically ferrocenyl substituted group V compounds. *J. Organomet. Chem.* **2013**, *743*, 97−101.

(16) Schulz, J.; Antala, J.; Císařová, I.; Štěpnička, P. Beyond phosphorus: synthesis, reactivity, coordination behaviour and catalytic properties of 1,1′-bis(diphenylstibino)ferrocene. *Dalton Trans.* **2023**, *52*, 1198−1211.

(17) (a) Gan, K.-S.; Hor, T. S. A. 1,1′-Bis(diphenylphosphino)-ferrocene. Coordination Chemistry, Organic Syntheses, and Catalysis. In *Ferrocenes: Homogeneous Catalysis, Organic Synthesis, Materials Science*; Togni, A., Hayashi, T., Eds.; Wiley-VCH: 1995; Chapter 1, pp 3−104. (b) Chien, S. W.; Hor, T. S. A. The Coordination and Homogeneous Catalytic Chemistry of 1,1′-Bis(diphenylphosphino)-ferrocene and its Chalcogenide Derivatives. In *Ferrocenes: Ligands, Materials and Biomolecules*; Štěpnička, P., Ed.; Wiley: 2008; Chapter 2, pp 33−116. (c) Colacot, T. J.; Parisel, S. Synthesis, Coordination Chemistry and Catalytic Use of dppf Analogs. In *Ferrocenes: Ligands, Materials and Biomolecules*; Štěpnička, P., Ed.; Wiley: 2008; Chapter 3, pp 117−140. (d) Bandoli, G.; Dolmella, A. Ligating ability of 1,1′-bis(diphenylphosphino)ferrocene: a structural survey (1994−1998). *Coord. Chem. Rev.* **2000**, *209*, 161−196. (e) Dey, S.; Pietschnig, R. Chemistry of sterically demanding dppf-analogs. *Coord. Chem. Rev.* **2021**, *437*, 213850.

https://doi.org/10.1021/acs.inorgchem.3c02075
Inorg. Chem. 2023, 62, 14028−14043

(18) Brunel, J. M.; Faure, B.; Maffei, M. Phosphane−boranes: synthesis, characterization and synthetic applications,. *Coord. Chem. Rev.* **1998**, *178*−*180*, 665−698.
(19) Brisset, H.; Gourdel, Y.; Pellon, P.; Le Corre, M. Phosphine-borane complexes; direct use in asymmetric catalysis. *Tetrahedron Lett.* **1993**, *34*, 4523−4526.
(20) (a) Estevan, F.; Lahuerta, P.; Latorre, J.; Peris, E.; García-Granda, S.; Gómez-Beltrán, F.; Aguirre, A.; Salvadó, M. A. Synthesis and electrochemical studies of new ferrocene-labelled dinuclear rhodium(II) complexes. Crystal structures of $[Rh_2(O_2CMe)_2\{[(C_6H_4)PhP(C_5H_4)]Fe(C_5H_5)\}_2(HO_2CMe)_2]$ and $[Rh_2(O_2CMe)_2\{[(C_6H_4)PhP(C_5H_4)]_2Fe\}(HO_2CMe)]\cdot CH_2Cl_2$. *J. Chem. Soc., Dalton Trans.* **1993**, 1681−1688. (b) Muller, A.; Otto, S.; Roodt, A. Rapid phosphorus(III) ligand evaluation utilising potassium selenocyanate. *Dalton Trans.* **2008**, 650−657.
(21) Donaghy, K. J.; Carroll, P. J.; Sneddon, L. G. Reactions of 1,1′-Bis(diphenylphosphino)ferrocene with Boranes, Thiaboranes, and Carboranes. *Inorg. Chem.* **1997**, *36*, 547−553.
(22) Štěpnička, P.; Císařová, I. Selective borane reduction of phosphinoferrocene carbaldehydes to phosphinoalcohol−borane adducts. The coordination behaviour of 1-(diphenylphosphino)-1′-(methoxymethyl)ferrocene, a new ferrocene O,P-hybrid donor prepared from such an adduct. *Dalton Trans.* **2013**, *42*, 3373−3389.
(23) (a) Lindner, C.; Maryasin, B.; Richter, F.; Zipse, H. Methyl cation affinity (MCA) for phosphanes. *J. Phys. Org. Chem.* **2010**, *23*, 1036−1042. (b) Lindner, C.; Tandon, R.; Maryasin, B.; Larionov, E.; Zipse, H. Cation affinity numbers of Lewis bases. *Beilstein J. Org. Chem.* **2012**, *8*, 1406−1442.
(24) Alkylation of triphenylstibine requires a stronger alkylating agent, e.g., the Meerwein salt: Henry, M. C.; Wittig, G. The Organometallic Alkylidene Reaction. *J. Am. Chem. Soc.* **1960**, *82*, 563−564.
(25) Kübler, P.; Sundermeyer, J. Ferrocenyl-phosphonium ionic liquids−synthesis, characterisation and electrochemistry. *Dalton Trans.* **2014**, *43*, 3750−3766.
(26) BH_3 scrambling was observed in ferrocene acylphosphines of the type $R_2PfcC(O)PR'_2$: Vosáhlo, P.; Císařová, I.; Štěpnička, P. Synthesis, coordination behavior, and catalytic properties of dppf congeners with an inserted carbonyl moiety. *New J. Chem.* **2022**, *46*, 21536−21552.
(27) Holmes, R. R.; Day, R. O.; Chandrasekhar, V.; Holmes, J. M. Pentacoordinated molecules. 67. Formation and structure of cyclic five-coordinated antimony derivatives. The first square-pyramidal geometry for a bicyclic stiborane. *Inorg. Chem.* **1987**, *26*, 157−163.
(28) Tofan, D.; Gabbaï, F. P. Fluorinated antimony(V) derivatives: strong Lewis acidic properties and application to the complexation of formaldehyde in aqueous solutions. *Chem. Sci.* **2016**, *7*, 6768−6778.
(29) (a) Arduengo, A. J., III; Stewart, C. A.; Davidson, F.; Dixon, D. A.; Becker, J. Y.; Culley, S. A.; Mizen, M. B. The Synthesis, Structure, and Chemistry of 10-Pn-3 Systems: Tricoordinate Hypervalent Pnictogen Compounds. *J. Am. Chem. Soc.* **1987**, *109*, 627−647. (b) Chishiro, A.; Akioka, I.; Sumida, A.; Oka, K.; Tohnai, N.; Yumura, T.; Imoto, H.; Naka, K. Tetrachlorocatecholates of triarylarsines as a novel class of Lewis acids. *Dalton Trans.* **2022**, *51*, 13716−13724.
(30) Štěpnička, P.; Horký, F. The coordination and catalytic chemistry of phosphanylferrocene chalcogenides. *Eur. J. Inorg. Chem.* **2022**, *2022*, No. e202200276.
(31) Kühl, O. *Phosphorus-31 NMR Spectroscopy: A Concise Introduction for the Synthetic Organic and Organometallic Chemist*; Springer: 2008.
(32) Baillie, C.; Zhang, L.; Xiao, J. Ferrocenyl Monophosphine Ligands: Synthesis and Applications in the Suzuki−Miyaura Coupling of Aryl Chlorides. *J. Org. Chem.* **2004**, *69*, 7779−7782.
(33) Verschoor-Kirss, M. J.; Hendricks, O.; Verschoor, C. M.; Conry, R.; Kirss, R. U. Chemical oxidation of ferrocenyl(phenyl)-phosphines and ferrocenyl(phenyl)phosphine chalcogenides. *Inorg. Chim. Acta* **2016**, *450*, 30−38.
(34) Beckmann, U.; Süslüyan, D.; Kunz, P. C. Is the $^1J_{PSe}$ Coupling Constant a Reliable Probe for the Basicity of Phosphines? A ^{31}P NMR Study. *Phosphorus, Sulfur, Silicon, Relat. Elem.* **2011**, *186*, 2061−2070.
(35) (a) Fang, Z.-G.; Hor, T. S. A.; Wen, Y.-S.; Liu, L.-K.; Mak, T. C. W. Molecular structures of 1,1′-bis(diphenylphosphino) ferrocene oxide and sulphide and their thermal properties. *Polyhedron* **1995**, *14*, 2403−2409. (b) Pilloni, G.; Longato, B.; Bandoli, G.; Corain, B. Bonding ability of 1,1′-bis(diphenylthiophosphoryl)ferrocene (dptpf) and its selenium analogue towards copper(I). Crystal structure of $[Cu(dptpf)]BF_4$. *J. Chem. Soc., Dalton Trans.* **1997**, 819−826.
(36) Selected examples: (a) Štěpnička, P.; Císařová, I. Synthesis of [1′-(diphenylthiophosphoryl)ferrocenyl]ethyne and alkyne-metal complexes thereof. *J. Organomet. Chem.* **2006**, *691*, 2863−2871. (b) Kahn, S. L.; Breheney, M. K.; Martinak, S. L.; Fosbenner, S. M.; Seibert, A. R.; Kassel, W. S.; Dougherty, W. G.; Nataro, C. Synthesis, Characterization, and Electrochemistry of Compounds Containing 1-Diphenylphosphino-1′-(di-tert-butylphosphino)ferrocene (dppdtbpf). *Organometallics* **2009**, *28*, 2119−2126. (c) Fernandes, T. A.; Solařová, H.; Císařová, I.; Uhlík, F.; Štícha, M.; Štěpnička, P. Synthesis of phosphinoferrocene amides and thioamides from carbamoyl chlorides and the structural chemistry of Group 11 metal complexes with these mixed-donor ligands. *Dalton Trans.* **2015**, *44*, 3092−3108. (d) Schulz, J.; Vosáhlo, P.; Uhlík, F.; Císařová, I.; Štěpnička, P. Probing the Influence of Phosphine Substituents on the Donor and Catalytic Properties of Phosphinoferrocene Carboxamides: A Combined Experimental and Theoretical Study. *Organometallics* **2017**, *36*, 1828−1841. (e) Vosáhlo, P.; Císařová, I.; Štěpnička, P. Comparing the asymmetric dppf-type ligands with their semi-homologous counterparts. *J. Organomet. Chem.* **2018**, *860*, 14−29.
(37) Mantina, M.; Chamberlin, A. C.; Valero, R.; Cramer, C. J.; Truhlar, D. G. Consistent van der Waals Radii for the Whole Main Group. *J. Phys. Chem. A* **2009**, *113*, 5806−5812.
(38) Cordero, B.; Gómez, V.; Platero-Prats, A. E.; Revés, M.; Echeverría, J.; Cremades, E.; Barragán, F.; Alvarez, S. Covalent radii revisited. *Dalton Trans.* **2008**, 2832−2838.
(39) Addison, A. W.; Rao, T. N.; Reedijk, J.; van Rijn, J.; Verschoor, G. C. Synthesis, structure, and spectroscopic properties of copper(II) compounds containing nitrogen−sulphur donor ligands; the crystal and molecular structure of aqua[1,7-bis(*N*-methylbenzimidazol-2′-yl)-2,6-dithiaheptane]copper(II) perchlorate. *J. Chem. Soc., Dalton Trans.* **1984**, 1349−1356.
(40) Gonzalez, V. M.; Park, G.; Yang, M.; Gabbai, F. Fluoride anion complexation and transport using a stibonium cation stabilized by an intramolecular P = O → Sb pnictogen bond. *Dalton Trans.* **2021**, *50*, 17897−17900.
(41) (a) Adeleke, J. A.; Liu, L.-K. Diphenylphosphinoferrocene. *Acta Crystallogr., Sect. C: Cryst. Struct. Commun.* **1993**, *49*, 680−682. (b) Kim, T.-J.; Lee, J.-H.; Kwon, S.-C.; Kwon, K.-H.; Uhm, J.-K.; Lee, H.; Byum, S.-I. Reaction and Coordination Chemistry of Ferrocenylphosphines with $(\eta^5\text{-}C_5H_5)Co(CO)_2$-Crystal structures of Two Ferrocenylphosphine Oxides. *Bull. Korean Chem. Soc.* **1991**, *12*, 116−118.
(42) Bader, R. F. W. A Quantum Theory of Molecular Structure and its Applications. *Chem. Rev.* **1991**, *91*, 893−928.
(43) Cremer, D.; Kraka, E. Chemical-Bonds without Bonding Electron-Density − Does the Difference Electron-Density Analysis Suffice for a Description of the Chemical-Bond? *Angew. Chem., Int. Ed. Engl.* **1984**, *23*, 627−628.
(44) (a) Hupf, E.; Lork, E.; Mebs, S.; Beckmann, J. Intramolecularly Coordinated (6-(Diphenylphosphino)acenaphth-5-yl)stannanes. Repulsion vs Attraction of P- and Sn-Containing Substituents in the *peri* Positions. *Organometallics* **2014**, *33*, 2409−2423. (b) Hupf, E.; Lork, E.; Mebs, S.; Checińska, L.; Beckmann, J. Probing Donor-Acceptor Interactions in peri-Substituted Diphenylphosphinoacenaphthyl-Element Dichlorides of Group 13 and 15 Elements. *Organometallics* **2014**, *33*, 7247−7259. (c) Hupf, E.; Do, T. G.; Nordheider, A.; Wehrhahn, M.; Sanz Camacho, P.; Ashbrook, S. E.; Lork, E.; Slawin, A. M. Z.; Mebs, S.; Woollins, J. D.; Beckmann, J. Selective Oxidation and Functionalization of 6-Diphenylphosphinoacenaphthyl-5-tellur-

https://doi.org/10.1021/acs.inorgchem.3c02075
Inorg. Chem. 2023, 62, 14028−14043

enyl Species 6-Ph_2P-Ace-5-TeX (X = Mes, Cl, O_3SCF_3). Various Types of P−E···Te(II,IV) Bonding Situations (E = O, S, Se). *Organometallics* **2017**, *36*, 1566−1579. (d) Mokrai, R.; Barrett, J.; Apperley, D. C.; Benkö, Z.; Heift, D. Tweaking the Charge Transfer: Bonding Analysis of Bismuth(III) Complexes with a Flexidentate Phosphane Ligand. *Inorg. Chem.* **2020**, *59*, 8916−8924.

(45) (a) Streitweiser, A., Jr; Rajca, A.; McDowell, R. S.; Glaser, R. Semipolar P−O and P−C Bonds: A Theoretical Study of Hypophosphite and Related Methylenephosphoranes. *J. Am. Chem. Soc.* **1987**, *109*, 4184−4188. (b) Chesnut, D. B. An Ab Initio Nuclear Magnetic Resonance and Atoms-in-Molecules Study of the PO Bond in Phosphine Oxides. *J. Am. Chem. Soc.* **1998**, *120*, 10504−10510. (c) Dobado, J. A.; Martínez-García, H.; Molina, J. M.; Sundberg, M. R. Chemical Bonding in Hypervalent Molecules Revised. Application of the *Atoms in Molecules Theory* to Y_3X and Y_3XZ (Y = H or CH_3; X = N, P or As; Z = O or S) Compounds. *J. Am. Chem. Soc.* **1998**, *120*, 8461−8471. (d) Chesnut, D. B.; Savin, A. The Electron Localization Function (ELF) Description of the PO Bond in Phosphine Oxide. *J. Am. Chem. Soc.* **1999**, *121*, 2335−2336. (e) Yamada, K.; Koga, N. Variationally Determined Electronic States for the Theoretical Analysis of Intramolecular Interaction. II. Qualitative Nature of the P−O Bond in Phosphine Oxides. *J. Comput. Chem.* **2013**, *34*, 149−161. (f) Yang, T.; Andrada, D. M.; Frenking, G. Dative *versus* electron-sharing bonding in N-oxides and phosphane oxides R_3EO and relative energies of the R_2EOR isomers (E = N, P; R = H, F, Cl, Me, Ph). A theoretical study. *Phys. Chem. Chem. Phys.* **2018**, *20*, 11856−11866. (g) Lindquist-Kleissler, B.; Wenger, J. S.; Johnstone, T. C. Analysis of Oxygen−Pnictogen Bonding with Full Bond Path Topological Analysis of the Electron Density. *Inorg. Chem.* **2021**, *60*, 1846−1856.

(46) Haaland, A.; Nilsson, J. E.; et al. The Determination of Barriers to Internal Rotation by Means of Electron Diffraction. Ferrocene and Ruthenocene. *Acta Chem. Scand.* **1968**, *22*, 2653−2670.

(47) Erdmann, P.; Leitner, J.; Schwarz, J.; Greb, L. An Extensive Set of Accurate Fluoride Ion Affinities for p-Block Element Lewis Acids and Basic Design Principles for Strong Fluoride Ion Acceptors. *ChemPhysChem* **2020**, *21*, 987−994.

(48) Calculated at the PW6B95(d3bj)/def2-qzvpp//PBE0(d3)/def2-TZVP:sdd(Fe,Sb) level of theory in vacuum at 298.15 K.

(49) (a) Knizia, G. Intrinsic Atomic Orbitals: An Unbiased Bridge between Quantum Theory and Chemical Concepts. *J. Chem. Theory Comput.* **2013**, *9*, 4834−4843. (b) Knizia, G.; Klein, J. E. M. N. Electron Flow in Reaction Mechanisms−Revealed from First Principles. *Angew. Chem., Int. Ed.* **2015**, *54*, 5518−5522.

(50) (a) Sandblom, N.; Ziegler, T.; Chivers, T. A density functional study of the bonding in tertiary phosphine chalcogenides and related molecules. *Can. J. Chem.* **1996**, *74*, 2363−2371. See also ref 45c.

(51) Yamada, K.; Koga, N. Variationally Determined Electronic States for the Theoretical Analysis of Intramolecular Interaction. II. Qualitative Nature of the P−O Bond in Phosphine Oxides. *J. Comput. Chem.* **2013**, *34*, 149−161.

(52) (a) Gritzner, G.; Kůta, J. Recommendations on reporting electrode potentials in nonaqueous solvents. *Pure Appl. Chem.* **1984**, *56*, 461−466. (b) Gagné, R. R.; Koval, C. A.; Lisensky, G. C. Ferrocene as an Internal Standard for Electrochemical Measurements. *Inorg. Chem.* **1980**, *19*, 2854−2855.

(53) (a) Pilloni, G.; Longato, B.; Corain, B. Heteropolymetallic complexes of 1,1′-bis(diphenylphosphino)ferrocene (dppf) VII. Redox behaviour of dppf. *J. Organomet. Chem.* **1991**, *420*, 57−65. (b) Zanello, P.; Opromolla, G.; Giorgi, G.; Sasso, G.; Togni, A. Redox behaviour of ferrocene derivatives VIII. 1,1′-Bis(diphenylphosphino)-ferrocenes. *J. Organomet. Chem.* **1996**, *506*, 61−65. (c) Nataro, C.; Campbell, A. N.; Ferguson, M. A.; Incarvito, C. D.; Rheingold, A. L. Group 10 metal complexes of 1,1′-bis(diphenylphosphino)ferrocene (dppf) and 1,1′-bis(diphenylphosphino)ruthenocene: A structural and electrochemical investigation. X-ray structures of $[MCl_2(dppr)]$ (M = Ni, Pd). *J. Organomet. Chem.* **2003**, *673*, 47−55.

(54) Representative examples: (a) Podlaha, J.; Štěpnička, P.; Ludvík, J.; Císařová, I. 1′-(Diphenylphosphino)ferrocenecarboxylic acid and Its *P*-Oxide and Methylester: Synthesis, Characterization, Crystal Structure, and Electrochemistry. *Organometallics* **1996**, *15*, 543−550. (b) Ghent, B. L.; Martinak, S. L.; Sites, L. A.; Golen, J. A.; Rheingold, A. L.; Nataro, C. Electrochemistry and complexation of Josiphos ligands. *J. Organomet. Chem.* **2007**, *692*, 2365−2374. (c) Bennett, M. A.; Bhargava, S. K.; Bond, A. M.; Burgar, I. M.; Guo, S.-X.; Kar, G.; Privér, S. H.; Wagler, J.; Willis, A. C.; Torriero, A. A. J. Synthesis, X-ray structure and electrochemical oxidation of palladium(II) complexes of ferrocenyldiphenylphosphine. *Dalton Trans.* **2010**, *39*, 9079−9090.

(55) (a) Swartz, B. D.; Nataro, C. Anodic Electrochemistry of Ferrocenylphosphine and Ruthenocenylphosphine Chalcogenide Complexes and Lewis Acid Adducts. *Organometallics* **2005**, *24*, 2447−2451 See also. (b) Barriere, F.; Kirss, R. U.; Geiger, W. E. Anodic Electrochemistry of Multiferrocenyl Phosphine and Phosphine Chalcogenide Complexes in Weakly Nucleophilic Electrolytes. *Organometallics* **2005**, *24*, 48−52.

(56) For a description and further examples of this approach, see: (a) Schulz, J.; Uhlík, F.; Speck, J. M.; Císařová, I.; Lang, H.; Štěpnička, P. Synthesis, Crystal Structures, and Electrochemical Behavior of Fe−Ru Heterobimetallic Complexes with Bridged Metallocene Units. *Organometallics* **2014**, *33*, 5020−5032. (b) Škoch, K.; Císařová, I.; Uhlík, F.; Štěpnička, P. Comparing the reactivity of isomeric phosphinoferrocene nitrile and isocyanide in Pd(ii) complexes: synthesis of simple coordination compounds vs. preparation of P-chelated insertion products and Fischer-type carbenes. *Dalton Trans.* **2018**, *47*, 16082−16101. (c) Škoch, K.; Schulz, J.; Císařová, I.; Štěpnička, P. Pd(II) Complexes with Chelating Phosphinoferrocene Diaminocarbene Ligands: Synthesis, Characterization, and Catalytic Use in Pd-Catalyzed Borylation of Aryl Bromides. *Organometallics* **2019**, *38*, 3060−3073. (d) Vosáhlo, P.; Schulz, J.; Císařová, I.; Štěpnička, P. Cyclopalladation of a ferrocene acylphosphine and the reactivity of the C−H activated products. *Dalton Trans.* **2021**, *50*, 6232−6244.

(57) Oxidation of stibine to a stiborane moiety has been shown to affect physical properties. For a representative example, see: Lo, Y.-H.; Gabbaï, F. P. Controlling the Properties of a 2,2′-bipy−Platinum Dichloride Complex via Oxidation of a Peripheral Stibine Moiety. *Organometallics* **2018**, *37*, 2500−2506.

(58) Rössler, K.; Rüffer, T.; Walfort, B.; Packheiser, R.; Holze, R.; Zharnikov, M.; Lang, H. Synthesis, characterization and electrochemical behavior of unsymmetric transition metal-terminated biphenyl ethynyl thiols. *J. Organomet. Chem.* **2007**, *692*, 1530−1545.

(59) The solution $^{13}C\{^1H\}$ NMR spectrum of **7** could not be obtained due to sample decomposition.

(60) Dunstan, S. P. C.; Healy, P. C.; Sobolev, A. N.; Tiekink, E. R. T.; White, A. H.; Williams, M. L. Isomorphism in the structural chemistry of two-coordinate adducts of diphenyl(2-formylphenyl)-phosphine and triphenylphosphine with gold(I) halides. *J. Mol. Struct.* **2014**, *1072*, 253−259.

(61) (a) Schmidbaur, H. The Aurophilicity Phenomenon: A Decade of Experimental Findings, Theoretical Concepts and Emerging Applications. *Gold Bull.* **2000**, *33*, 3−10. (b) Schmidbaur, H.; Schier, A. A briefing on aurophilicity. *Chem. Soc. Rev.* **2008**, *37*, 1931−1951. (c) Schmidbaur, H.; Schier, A. Aurophilic interactions as a subject of current research: an up-date. *Chem. Soc. Rev.* **2012**, *41*, 370−412.

(62) (a) Steed, K. M.; Steed, J. W. Packing Problems: High Z' Crystal Structures and Their Relationship to Cocrystals, Inclusion Compounds, and Polymorphism. *Chem. Rev.* **2015**, *115*, 2895−2933. (b) Taylor, R.; Cole, J. C.; Groom, C. R. Molecular Interactions in Crystal Structures with $Z' > 1$. *Cryst. Growth Des.* **2016**, *16*, 2988−3001.

(63) Cambridge Structural Database, version 5.34 of November 2021, with updates from March, June and September 2022.

(64) For an example of an Au(I)-ferrocenebisphosphole complex, where aurophilic interactions give rise to a different polymorph, see: Orthaber, A.; Borucki, S.; Shen, W.; Réau, R.; Lescop, C.; Pietschnig, R. Coordination Behaviour of a Hexadentate1,1′-Ferrocenylene-

https://doi.org/10.1021/acs.inorgchem.3c02075
Inorg. Chem. 2023, 62, 14028−14043

Bridged Bisphosphole towards CoinageMetal Centres. *Eur. J. Inorg. Chem.* **2014**, *2014*, 1751−1759.
(65) Complex **11** was not included in catalytic testing because of facile hydrolysis of the catecholato-stiborane moiety that could influence the catalytic results.
(66) (a) Hashmi, A. S. K.; Weyrauch, J. P.; Frey, W.; Bats, J. W. Gold Catalysis: Mild Conditions for the Synthesis of Oxazoles from *N*-Propargylcarboxamides and Mechanistic Aspects. *Org. Lett.* **2004**, *6*, 4391−4394. (b) Weyrauch, J. P.; Hashmi, A. S. K.; Schuster, A.; Hengst, T.; Schetter, S.; Littmann, A.; Rudolph, M.; Hamzic, M.; Visus, J.; Rominger, F.; Frey, W.; Bats, J. W. Cyclization of Propargylic Amides: Mild Access to Oxazole Derivatives. *Chem. Eur. J.* **2010**, *16*, 956−963.
(67) Bárta, O.; Císařová, I.; Schulz, J.; Štěpnička, P. Assessing the influence of phosphine substituents on the catalytic properties of self-stabilised digold(I) complexes with supporting ferrocene phosphino-nitrile ligands. *New J. Chem.* **2019**, *43*, 11258−11262.
(68) Vosáhlo, P.; Štěpnička, P. Assessing the role of substituents in ferrocene acylphosphines and their impact on gold-catalysed reactions. *New J. Chem.* **2023**, *47*, 4510−4520.
(69) He, W.; Li, C.; Zhang, L. An Efficient [2 + 2 + 1] Synthesis of 2,5-Disubstituted Oxazoles via Gold-Catalyzed Intermolecular Alkyne Oxidation. *J. Am. Chem. Soc.* **2011**, *133*, 8482−8485.
(70) Astruc, D. Why is Ferrocene so Exceptional? *Eur. J. Inorg. Chem.* **2017**, *2017*, 6−29.

https://doi.org/10.1021/acs.inorgchem.3c02075
Inorg. Chem. 2023, 62, 14028−14043